Non-equilibrium critical behavior in brain simulations (GPUday 2026)

Géza Ódor, Shengfeng Deng, Istvan Papp, EK-MFA, Budapest

Gustavo Deco Barcelona UPF, Jeffrey Kelling Dresden HZDR

Non-equilibrium critical behavior in brain simulations (GPUday 2026)

Géza Ódor, Shengfeng Deng, Istvan Papp, EK-MFA, Budapest

Gustavo Deco Barcelona UPF, Jeffrey Kelling Dresden HZDR

Theoretical research and experiments suggest that the brain operates at or near a **critical state** between sustained activity and an inactive phase, exhibiting optimal computational properties (see: *Beggs & Plenz J. Neurosci. 2003; Chialvo Nat. Phys. 2010; Haimovici et al. PRL 2013*)

Non-equilibrium critical behavior in brain simulations (GPUday 2026)

Géza Ódor, Shengfeng Deng, Istvan Papp, EK-MFA, Budapest

Gustavo Deco Barcelona UPF, Jeffrey Kelling Dresden HZDR

Theoretical research and experiments suggest that the brain operates at or near a **critical state** between sustained activity and an inactive phase, exhibiting optimal computational properties (see: *Beggs & Plenz J. Neurosci. 2003; Chialvo Nat. Phys. 2010; Haimovici et al. PRL 2013*)

Neurons exhibit oscillatory behavior

Non-equilibrium critical behavior in brain simulations (GPUday 2026)

Géza Ódor, Shengfeng Deng, Istvan Papp, EK-MFA, Budapest

Gustavo Deco Barcelona UPF, Jeffrey Kelling Dresden HZDR

Theoretical research and experiments suggest that the brain operates at or near a **critical state** between sustained activity and an inactive phase, exhibiting optimal computational properties (see: *Beggs & Plenz J. Neurosci. 2003; Chialvo Nat. Phys. 2010; Haimovici et al. PRL 2013*)

Neurons exhibit oscillatory behavior

→ Synchronization criticality in brain models **?**

Phase transitions and criticality

Phase transitions and criticality

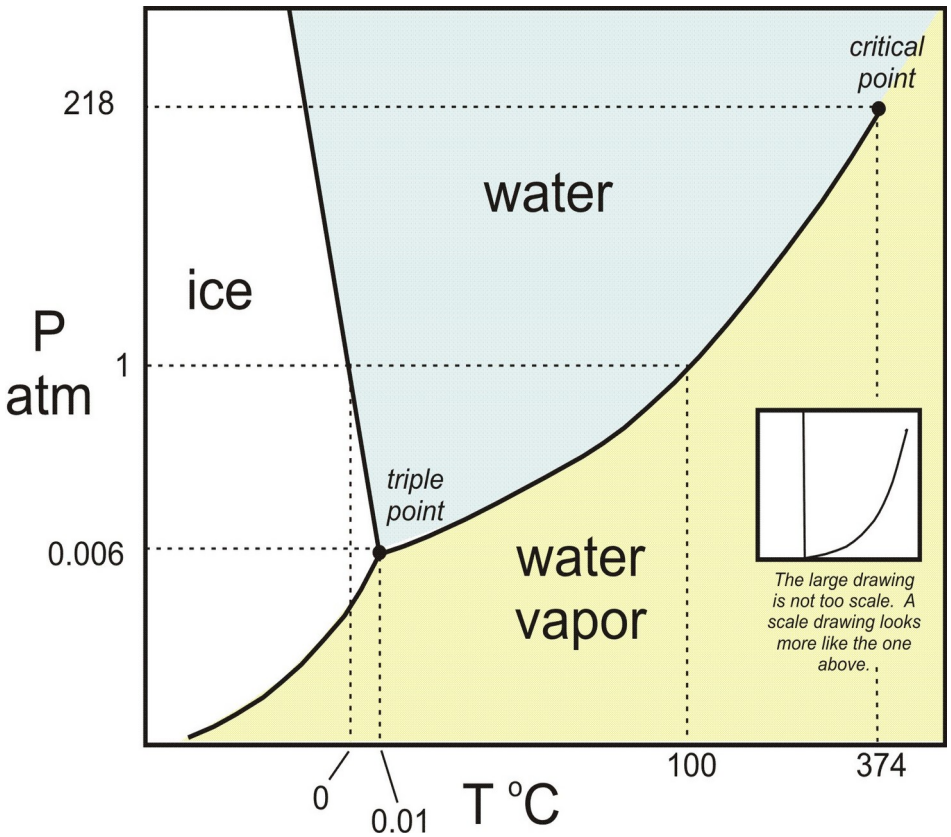

Phase transitions and criticality

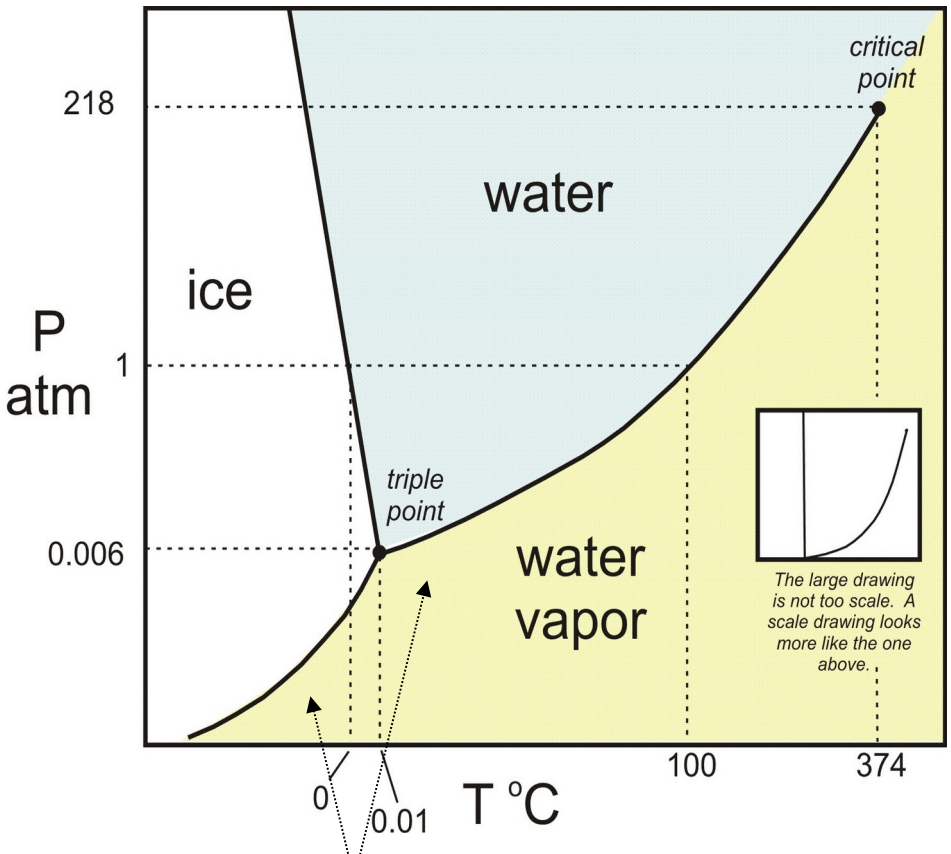

First order transitions

Phase transitions and criticality

Second order, continuous transition

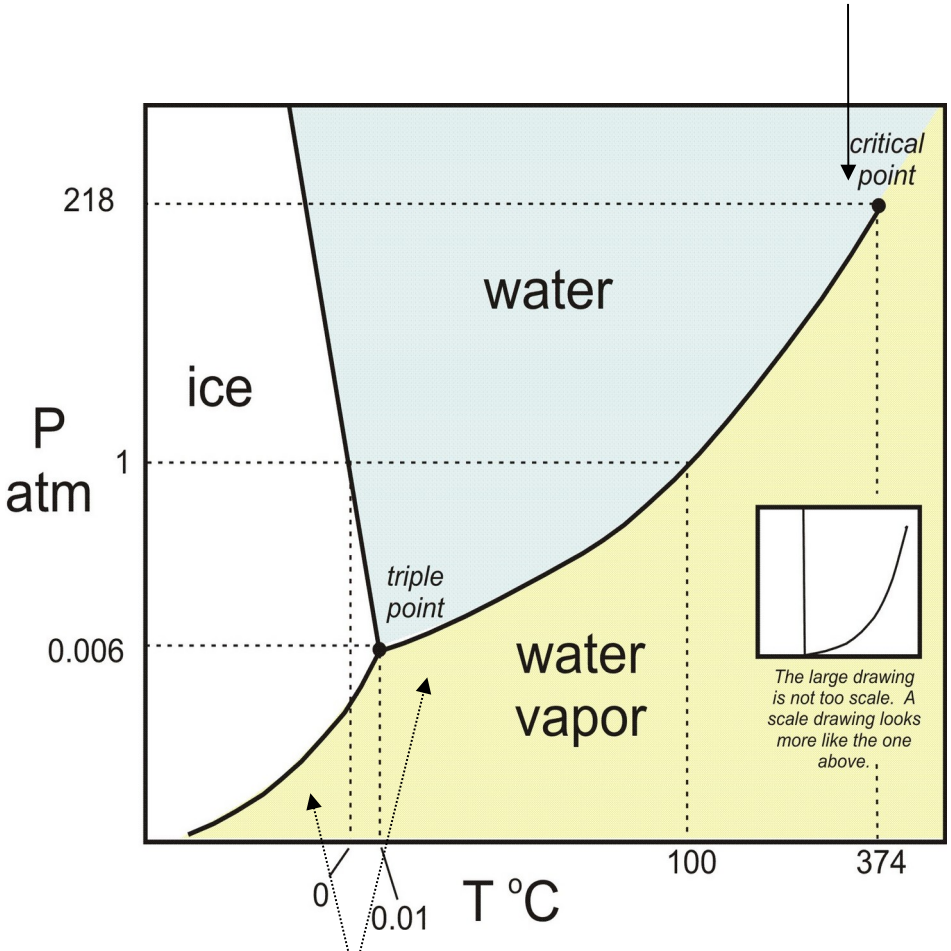

First order transitions

Phase transitions and criticality

Second order, continuous transition

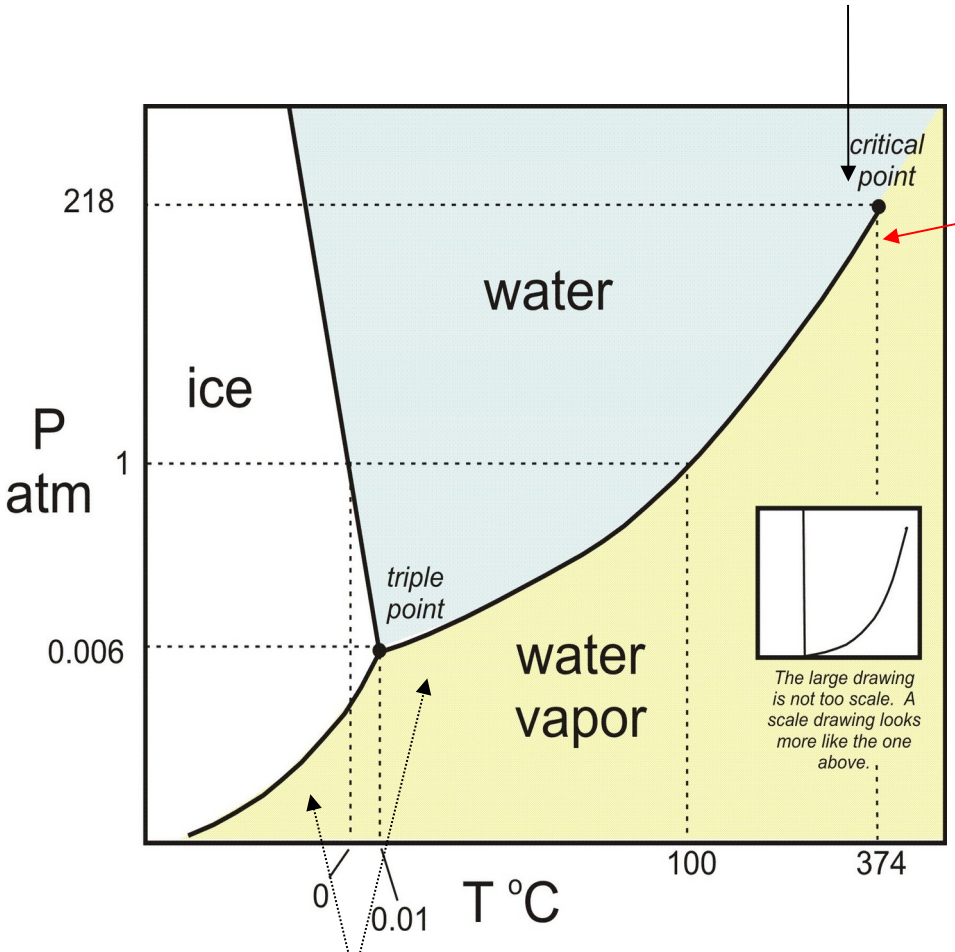

First order transitions

At the critical point:

Strong fluctuations

Phase transitions and criticality

Second order, continuous transition

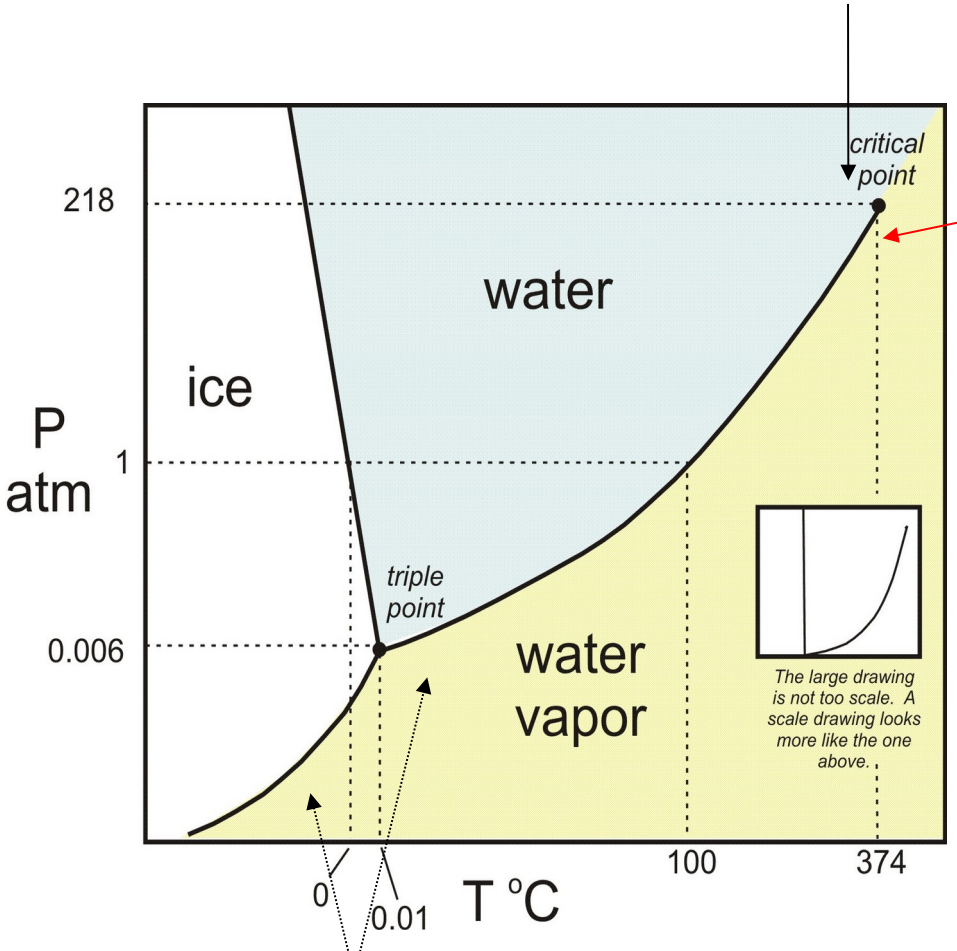

First order transitions

At the critical point:

Strong fluctuations

Diverging correlations:

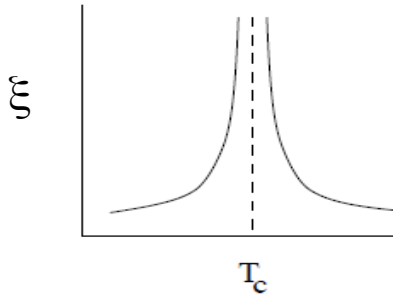

Phase transitions and criticality

Second order, continuous transition

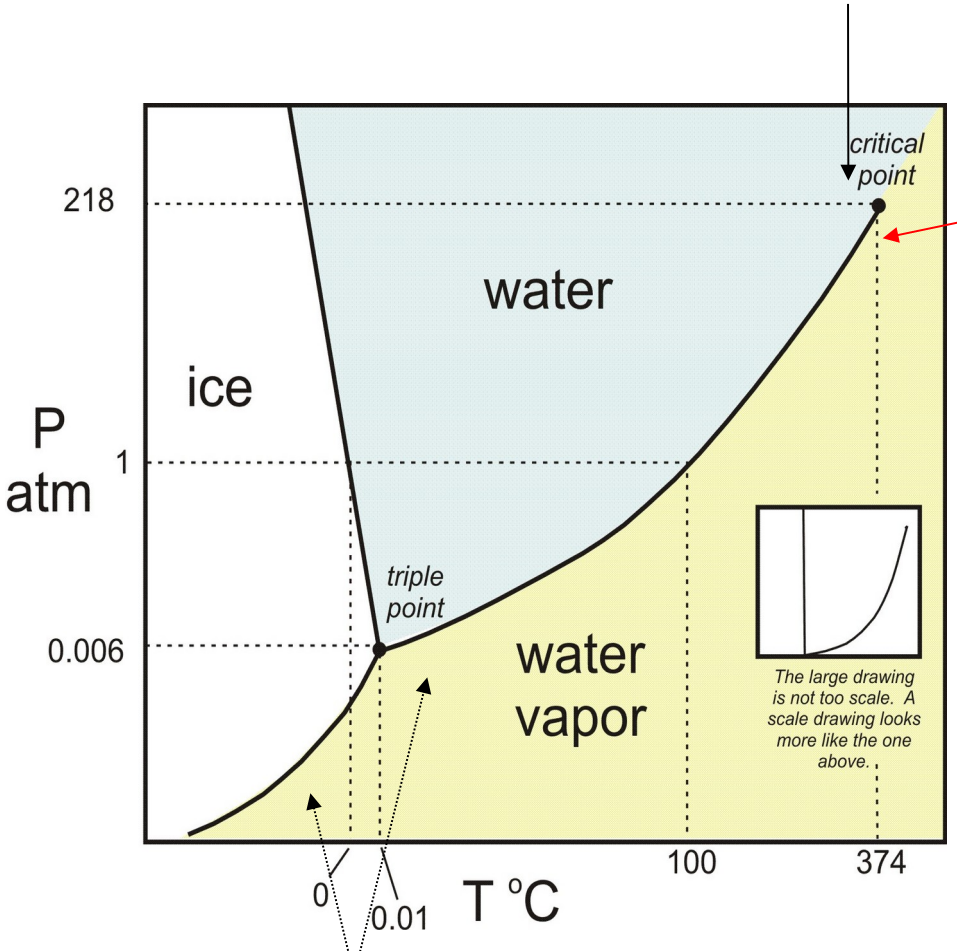

First order transitions

At the critical point:

Strong fluctuations

Diverging correlations:

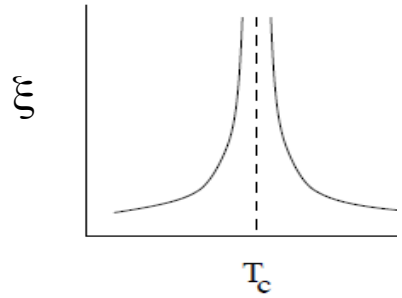

Rescaling invariance
(scale-free behavior):

$r \to br, \quad F(r,t,...) \to a^x F(br, b^z t, ...)$

Phase transitions and criticality

Second order, continuous transition

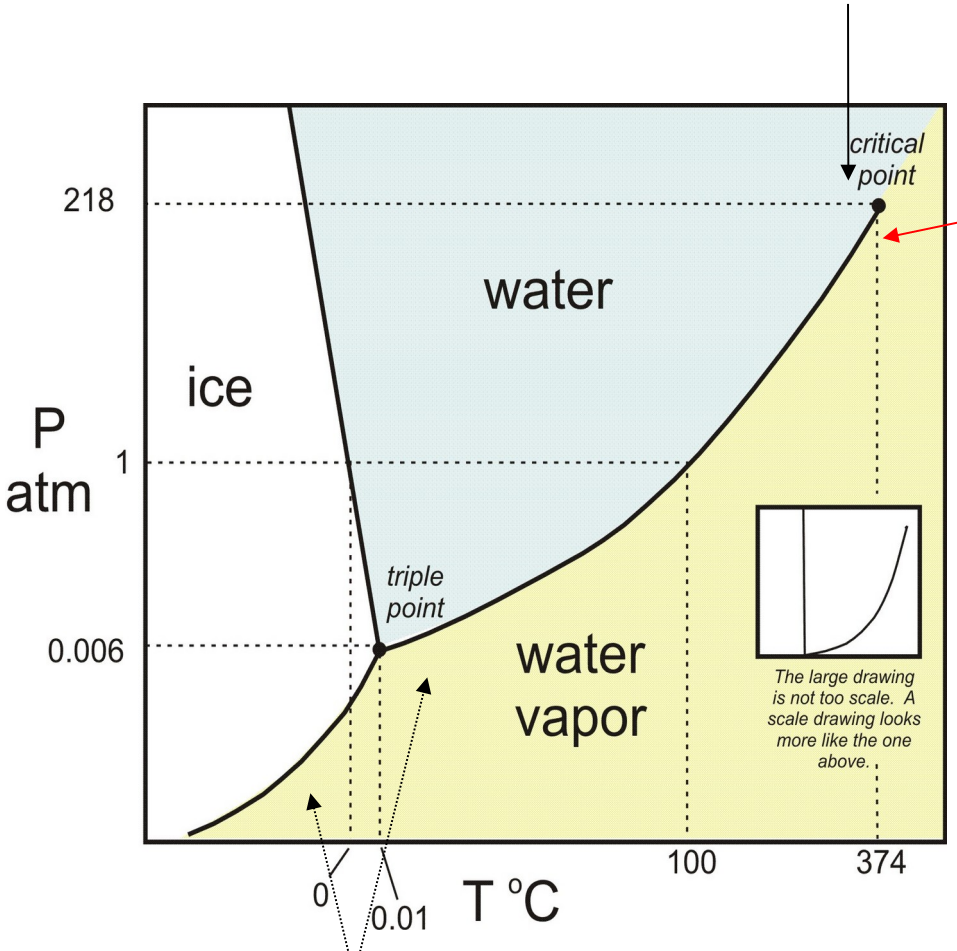

First order transitions

At the critical point:

Strong fluctuations

Diverging correlations:

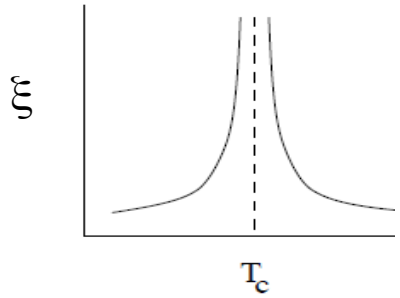

Rescaling invariance (scale-free behavior):

$r \rightarrow br, \quad F(r,t,...) \rightarrow a^x F(br, b^z t, ...)$

Power-laws: i.e. specific heat:

$$C_{\pm} = \frac{\partial E}{\partial T} \propto |t|^{\alpha_{\pm}}$$

Phase transitions and criticality

Second order, continuous transition

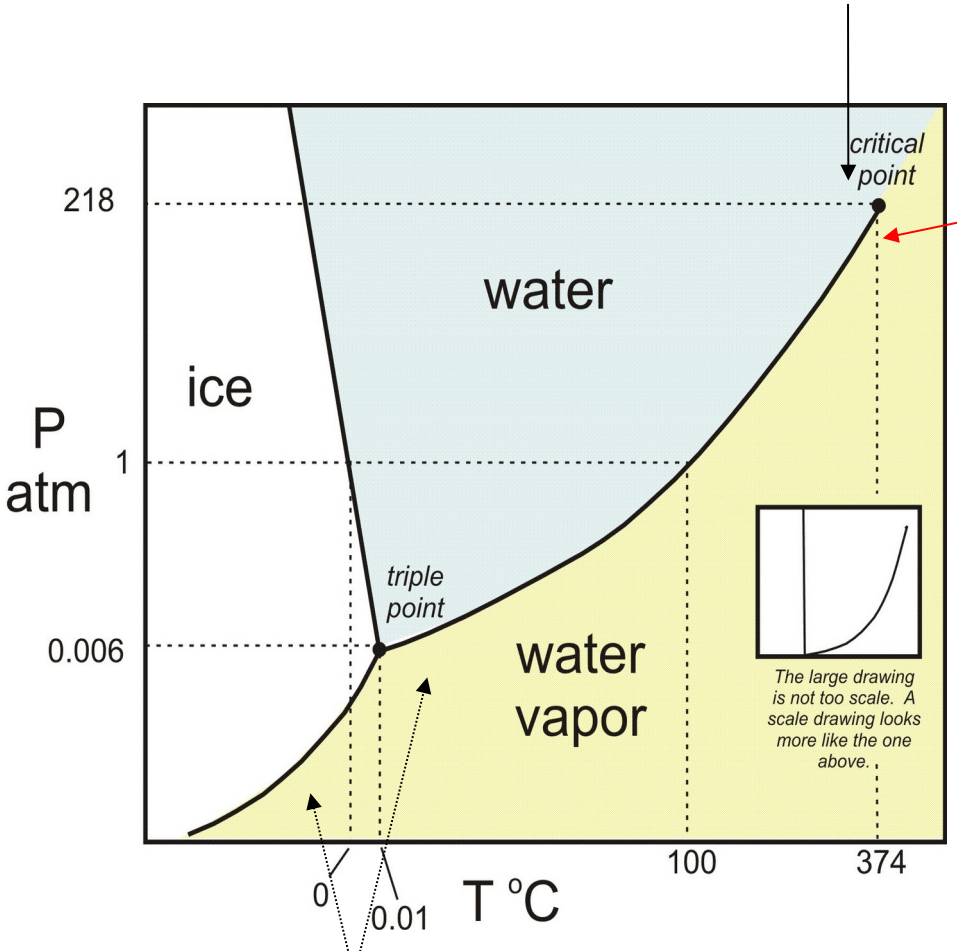

First order transitions

At the critical point:

Strong fluctuations

Diverging correlations:

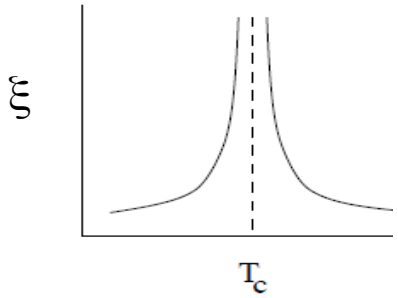

Rescaling invariance
(scale-free behavior):

$r \rightarrow br, \quad F(r,t,...) \rightarrow a^x F(br, b^z t, ...)$

Power-laws: i.e. specific heat:

$$C_{\pm} = \frac{\partial E}{\partial T} \propto |t|^{\alpha_{\pm}}$$

$$\chi_{\pm}(T, H \rightarrow 0^+) = \left.\frac{\partial m}{\partial H}\right|_{H=0^+} \propto |t|^{-\gamma_{\pm}}$$

susceptibility, autocorrelation ...

Phase transitions and criticality

Second order, continuous transition

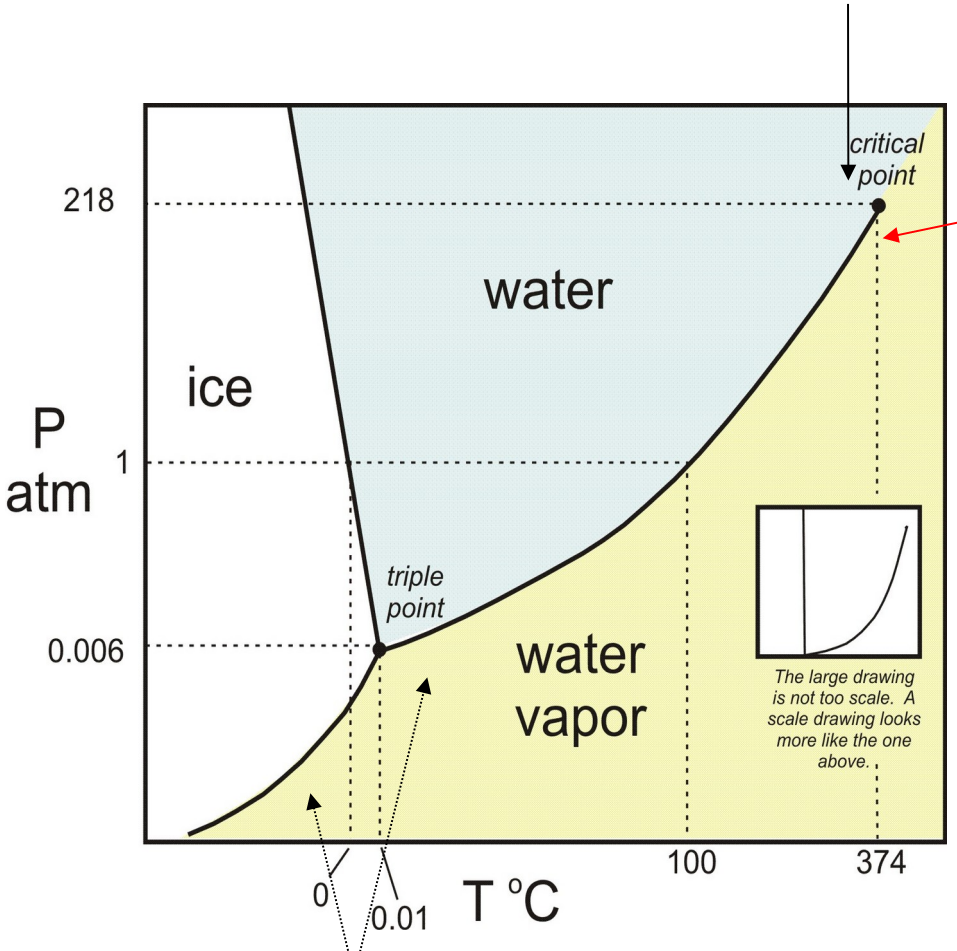

First order transitions

Universality !
Mean-field for d → ∞

At the critical point:

Strong fluctuations

Diverging correlations:

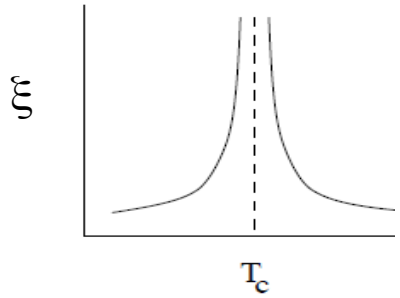

Rescaling invariance
(scale-free behavior):

$r \to br, \quad F(r,t,...) \to a^x F(br, b^z t, ...)$

Power-laws: i.e. specific heat:

$$C_\pm = \frac{\partial E}{\partial T} \propto |t|^{\alpha_\pm}$$

$$\chi_\pm(T, H \to 0^+) = \left.\frac{\partial m}{\partial H}\right|_{H=0^+} \propto |t|^{-\gamma_\pm}$$

susceptibility, autocorrelation ...

Brain experiments suggest near critical behavior

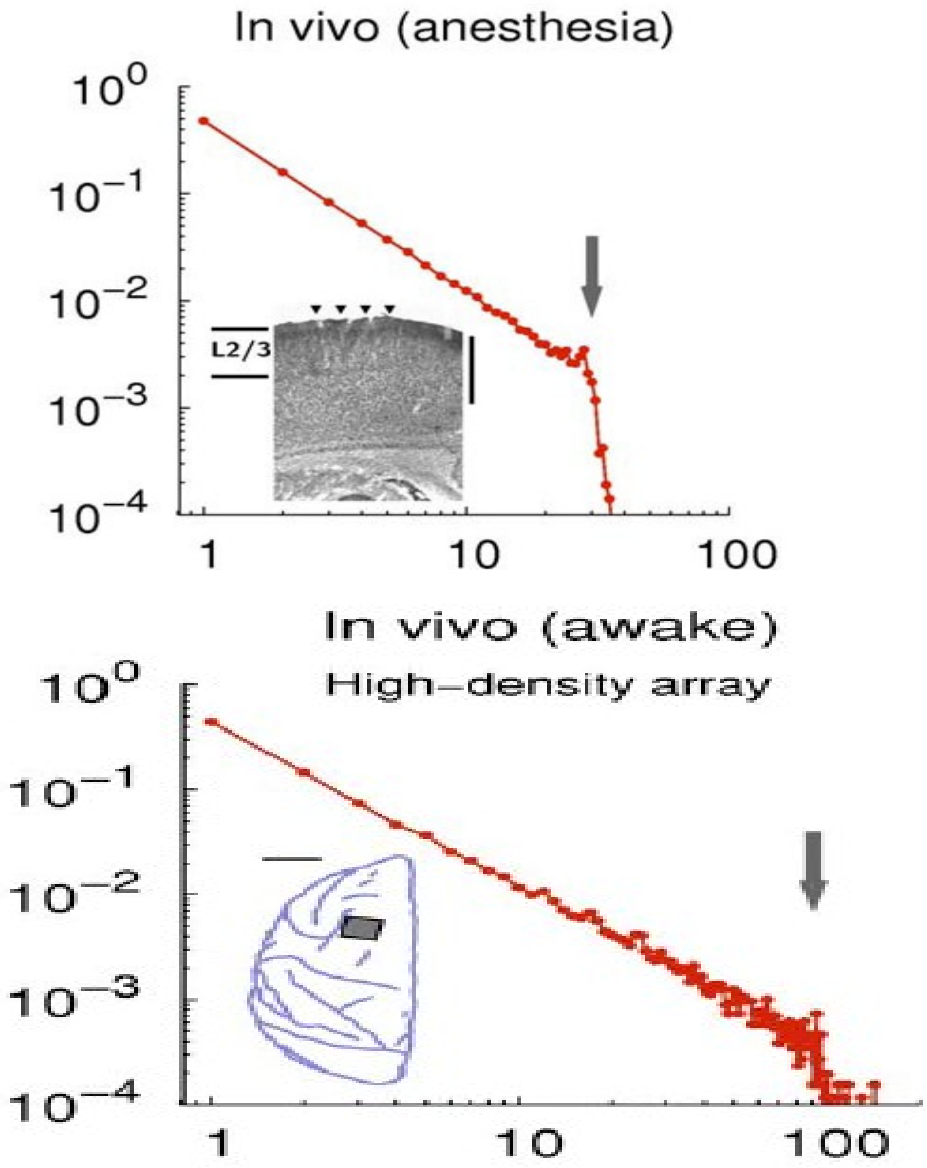

Brain experiments suggest near critical behavior

Electrode LFP experiments

Since Beggs and Plenz 2003

For humans and animals

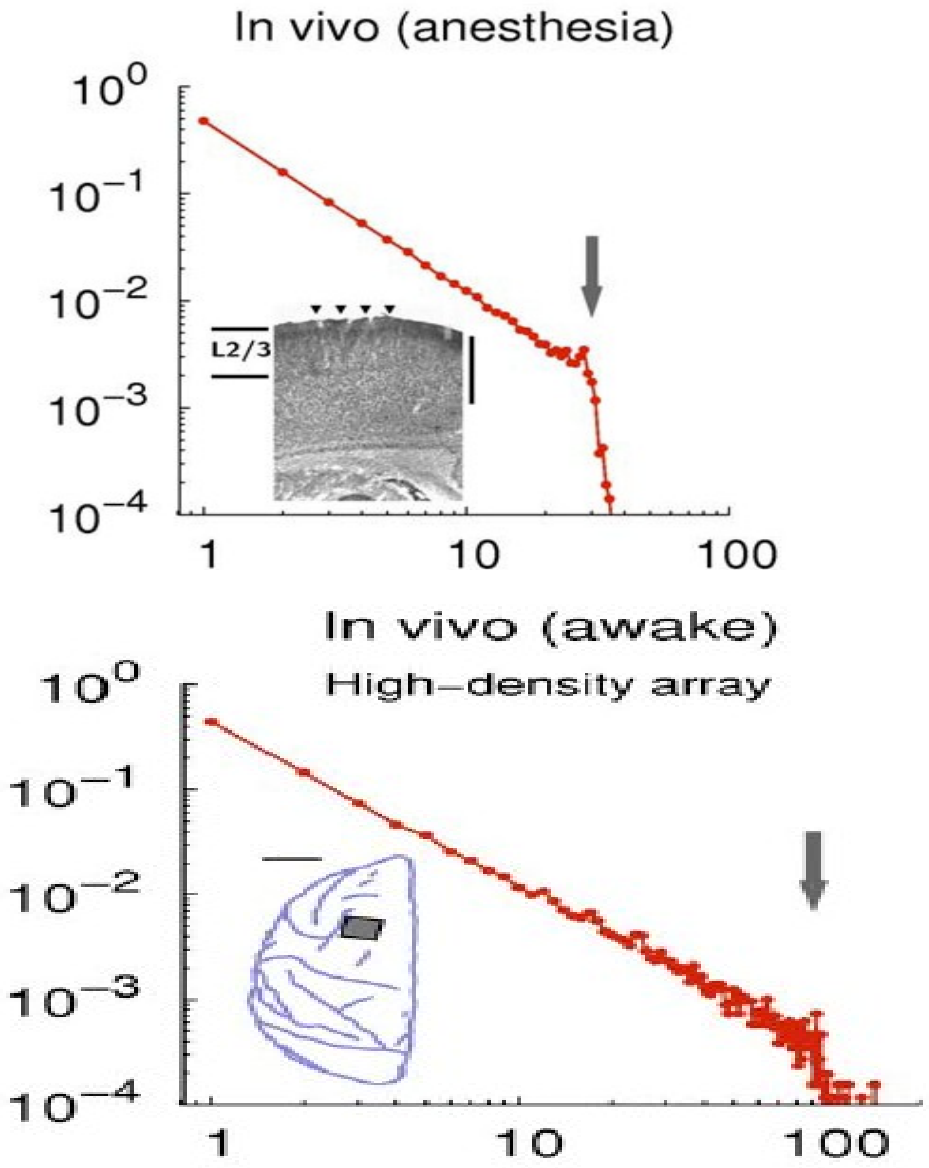

Brain experiments suggest near critical behavior

Electrode LFP experiments

Since Beggs and Plenz 2003

For humans and animals

In vitro, for balanced excitatory/inhibitory states

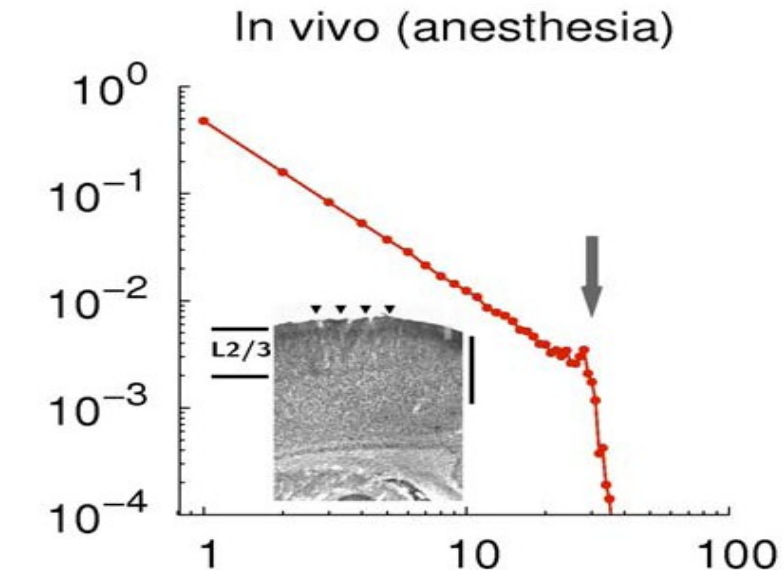

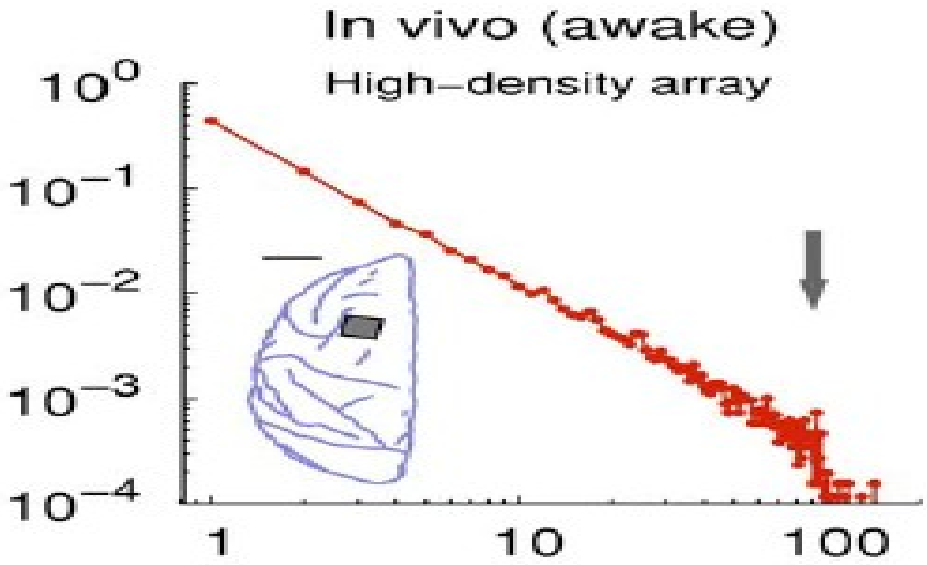

Brain experiments suggest near critical behavior

Electrode LFP experiments

Since Beggs and Plenz 2003

For humans and animals

In vitro, for balanced excitatory/inhibitory states

Other experiments: fMRI, BOLD,

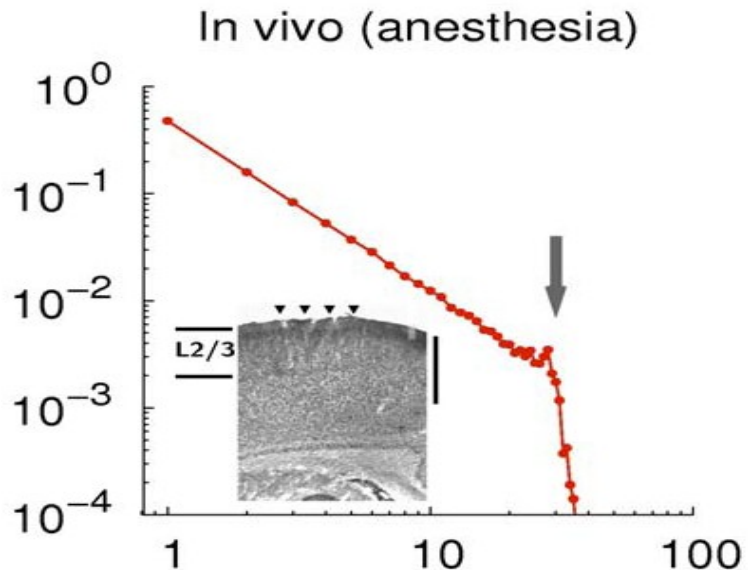

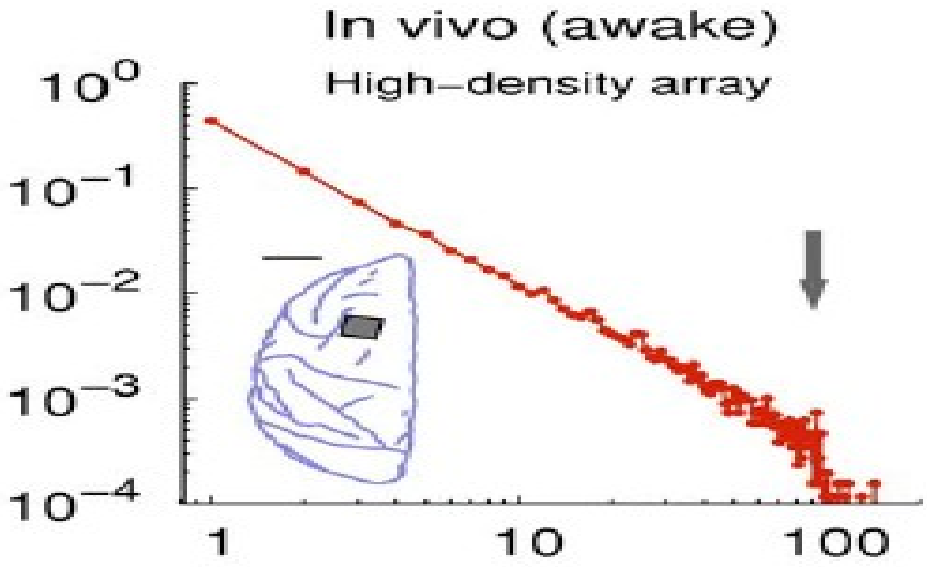

Brain experiments suggest near critical behavior

Electrode LFP experiments

Since Beggs and Plenz 2003

For humans and animals

In vitro, for balanced excitatory/inhibitory states

Other experiments: fMRI, BOLD, Voltage imaging, calcium imaging, MEG, EEG, **L**ong-**R**ange **T**emporal **C**orrelations (**LRTC**).

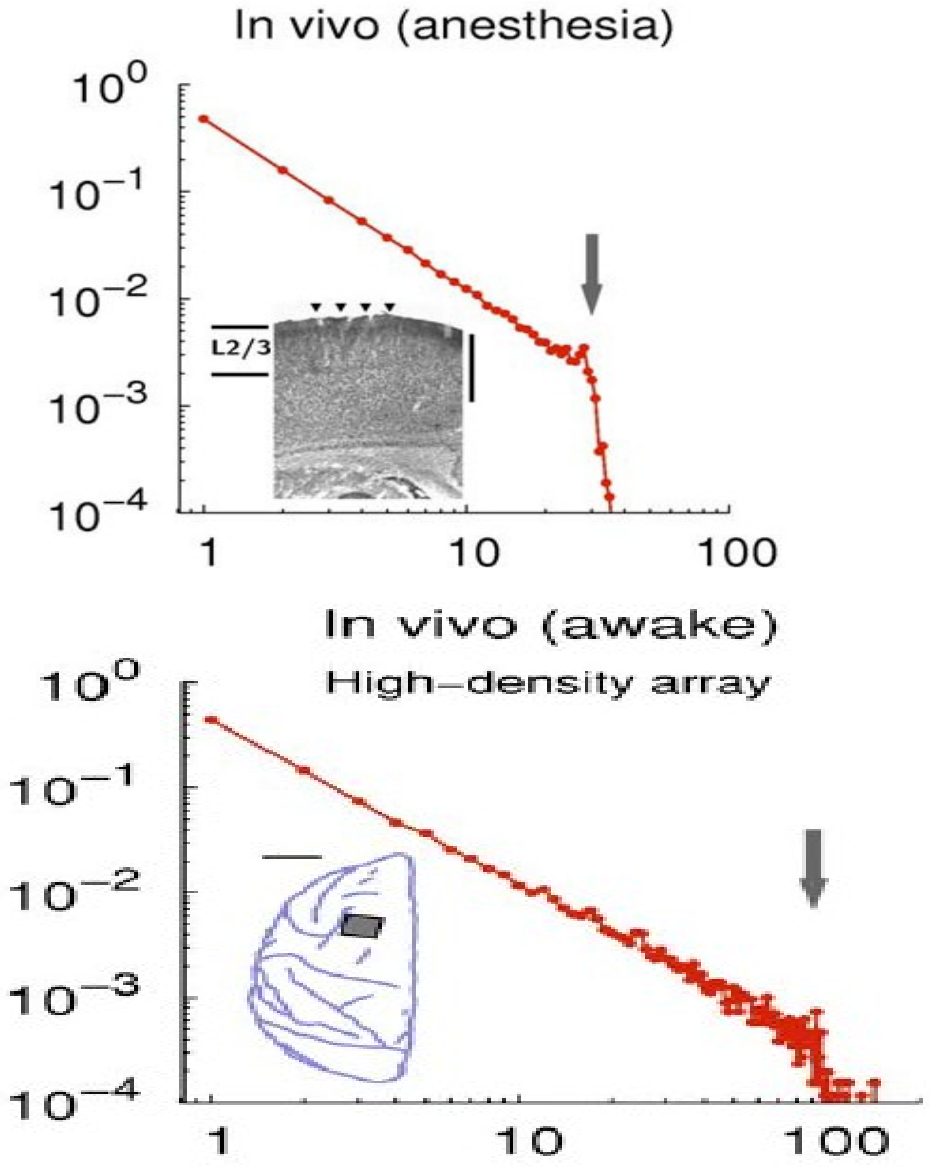

Brain experiments suggest near critical behavior

Electrode LFP experiments

Since Beggs and Plenz 2003

For humans and animals

In vitro, for balanced excitatory/inhibitory states

Other experiments: fMRI, BOLD, Voltage imaging, calcium imaging, MEG, EEG, **L**ong-**R**ange **T**emporal **C**orrelations (**LRTC**).

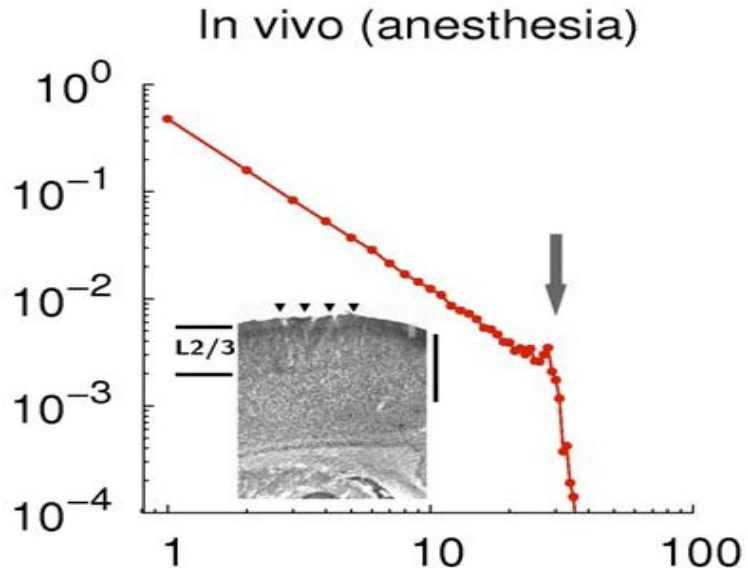

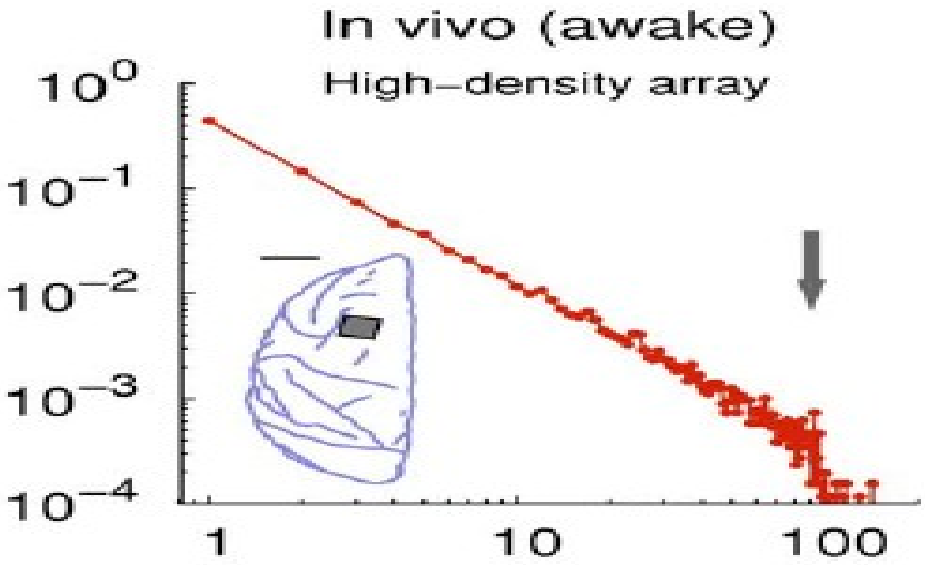

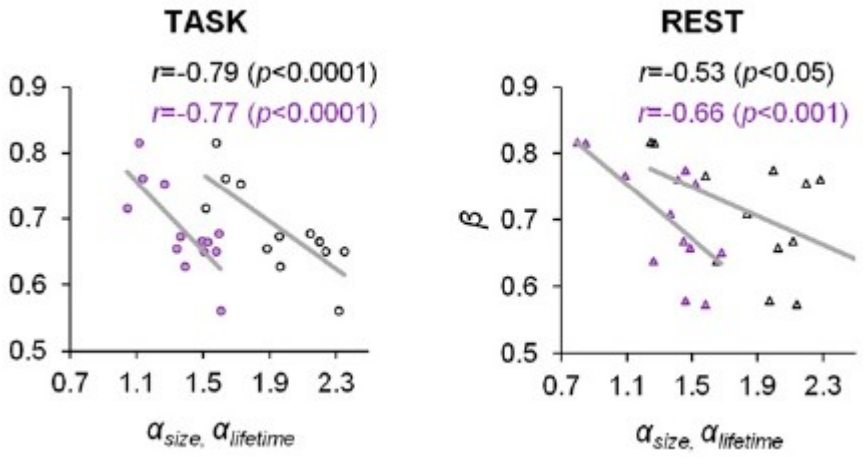

Brain experiments suggest near critical behavior

Electrode LFP experiments

Since Beggs and Plenz 2003

For humans and animals

In vitro, for balanced excitatory/inhibitory states

Other experiments: fMRI, BOLD, Voltage imaging, calcium imaging, MEG, EEG, **L**ong-**R**ange **T**emporal **C**orrelations (**LRTC**).

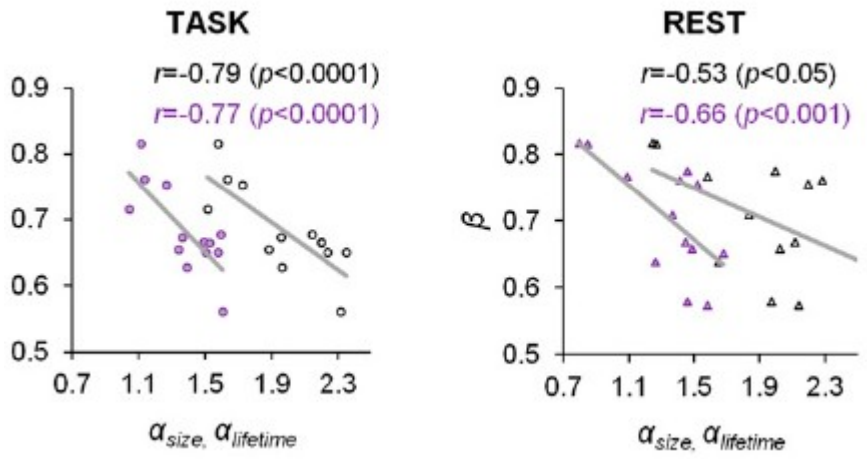

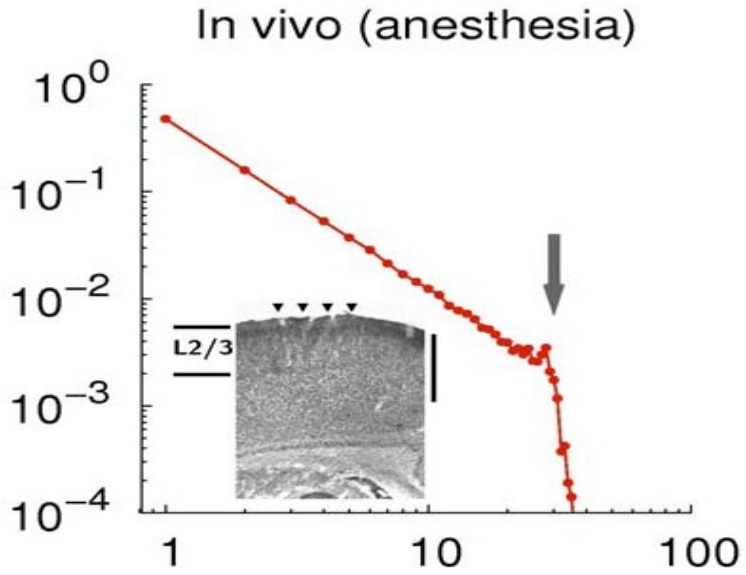

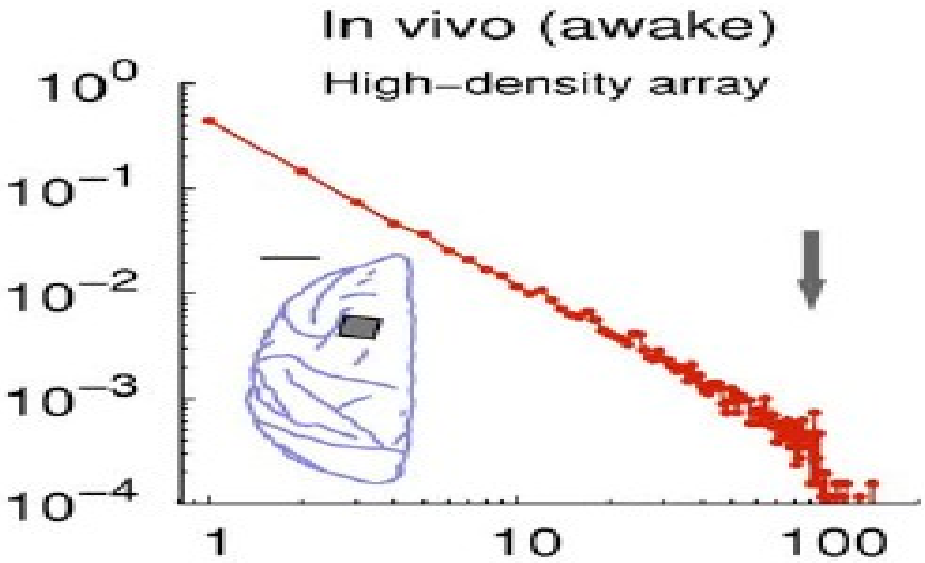

Nonuniversal critical exponents or Mean-field values : $\tau = 1.5$ $\tau_t = 2$?

Why would the brain be critical ?

Why would the brain be critical ?

Pros:

Diverging fluctuations →
High sensitivity to stimuli

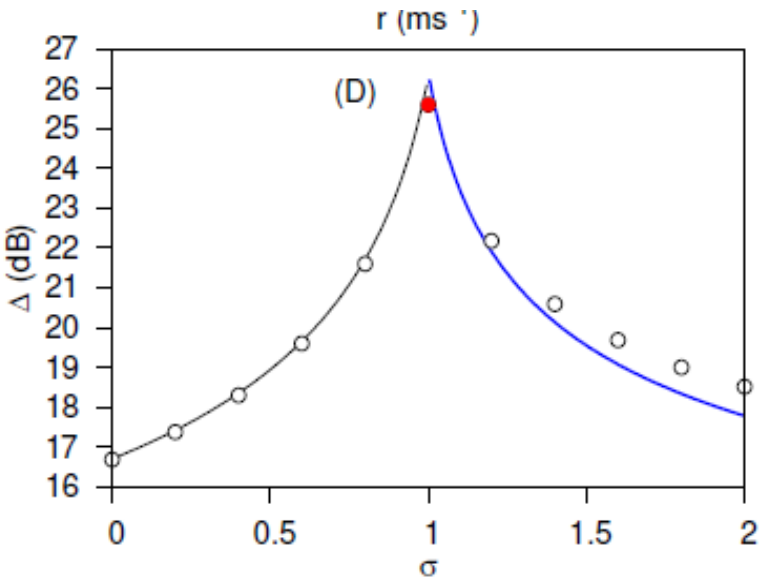

Why would the brain be critical ?

Pros:

Diverging fluctuations →
High sensitivity to stimuli

Diverging correlation functions →
Optimal transmission and
storage of information

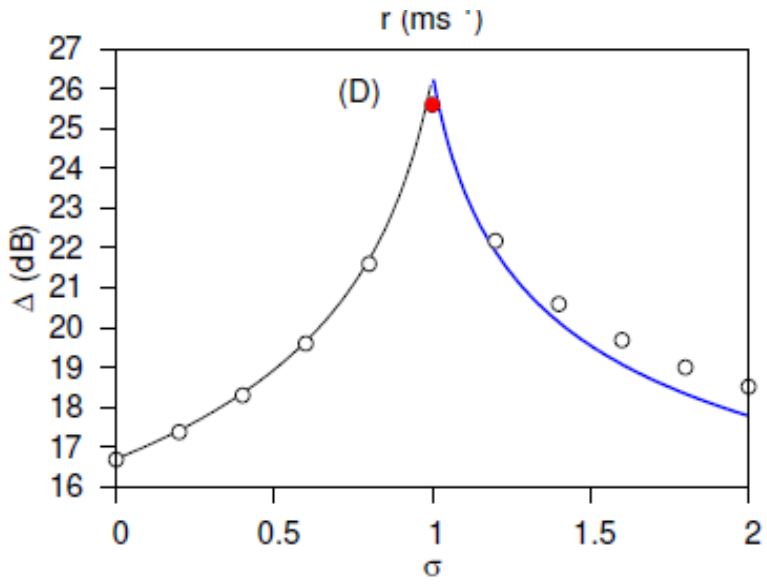

Why would the brain be critical ?

Pros:

Diverging fluctuations →
High sensitivity to stimuli

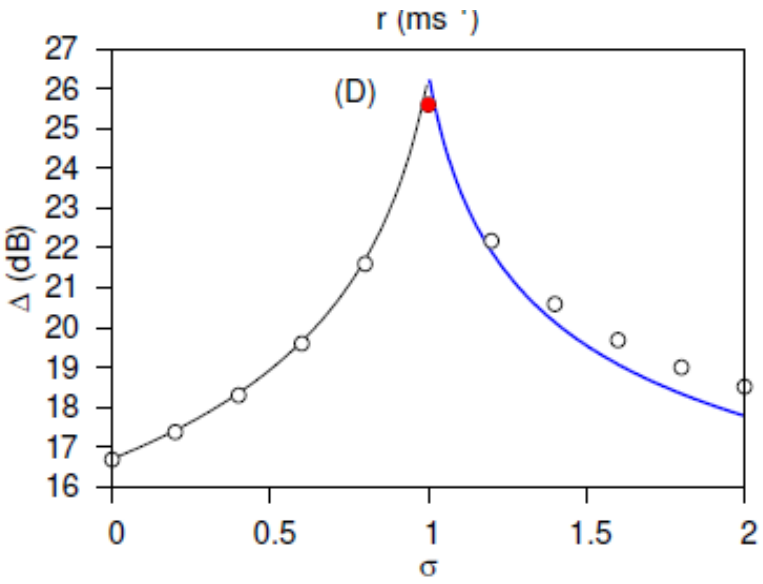

Diverging correlation functions →
Optimal transmission and
storage of information

Maximal information processing and computational performance → **AI?**

Why would the brain be critical ?

Pros:

Diverging fluctuations →
High sensitivity to stimuli

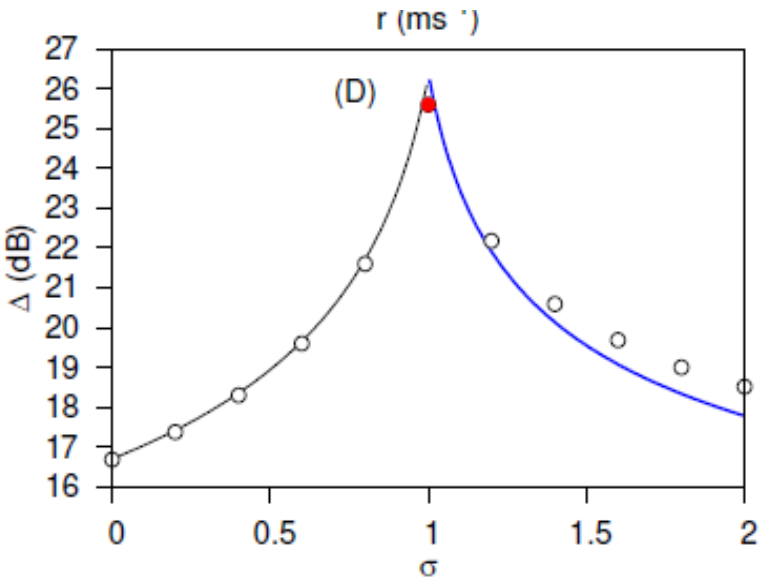

Diverging correlation functions →
Optimal transmission and
storage of information

Maximal information processing and computational performance
→ **AI?**

Cons: Tuning to critical point is needed
Danger of super-critical (epileptic) behavior

Why would the brain be critical ?

Pros:

Diverging fluctuations →
High sensitivity to stimuli

Diverging correlation functions →
Optimal transmission and
storage of information

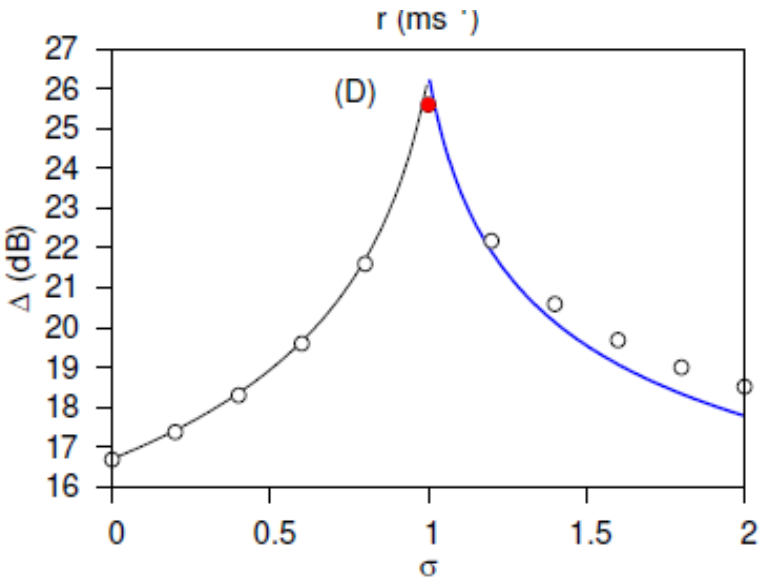

Maximal information processing and computational performance → **AI?**

Cons: Tuning to critical point is needed
Danger of super-critical (epileptic) behavior

Self-organization to criticality (SOC) ?

HUN REN

Kuramoto oscillator model (1975)

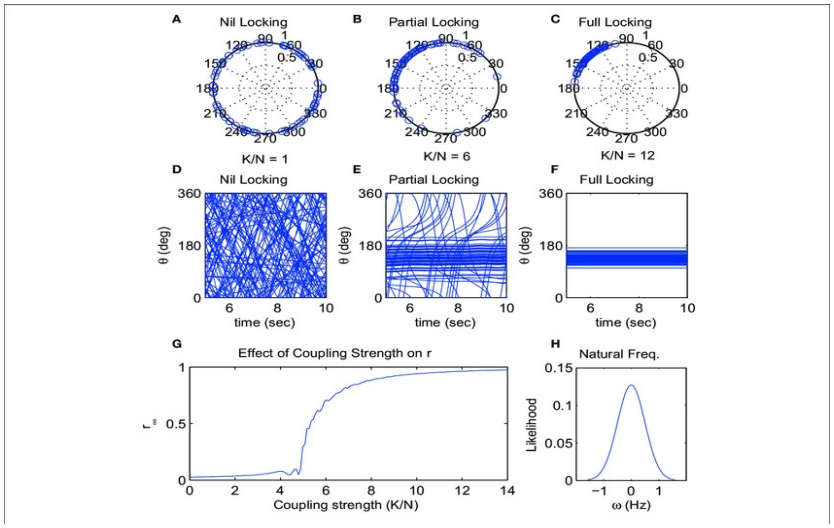

Kuramoto oscillator model (1975)

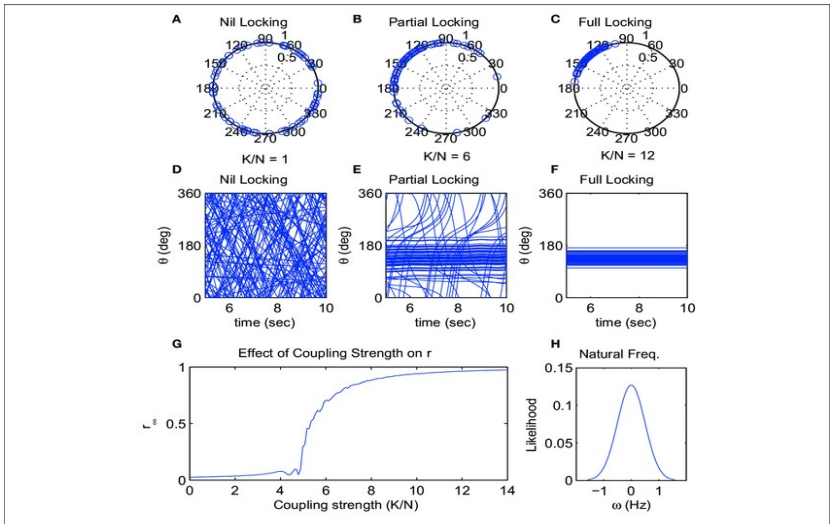

$$\dot{\theta}_i(t) = \omega_{i,0} + \frac{K}{k_i} \sum_j W_{ij} \sin[\theta_i(t) - \theta_j(t)]$$

Kuramoto oscillator model (1975)

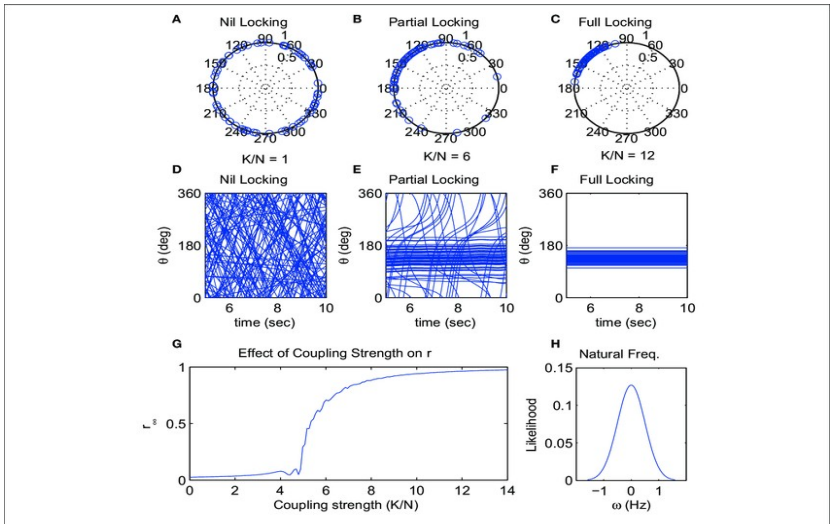

$$\dot{\theta}_i(t) = \omega_{i,0} + \frac{K}{k_i} \sum_j W_{ij} \sin[\theta_i(t) - \theta_j(t)]$$

phases $\theta_i(t)$

Kuramoto oscillator model (1975)

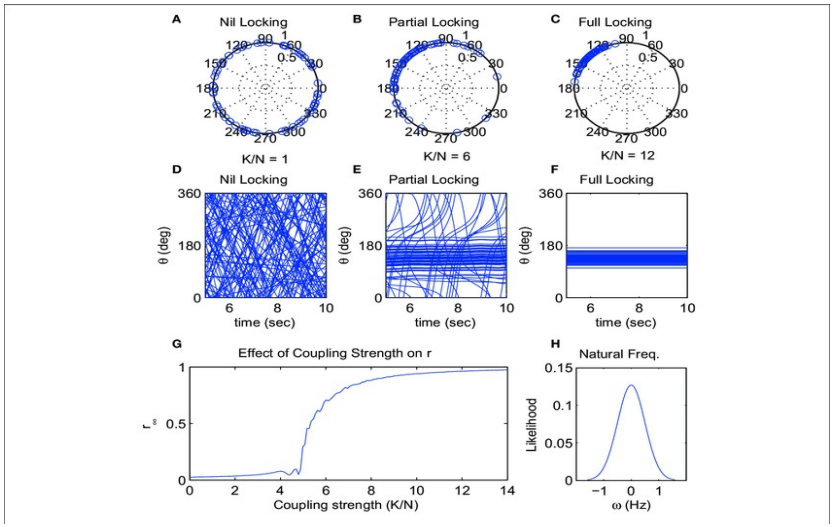

$$\dot{\theta}_i(t) = \omega_{i,0} + \frac{K}{k_i} \sum_j W_{ij} \sin[\theta_i(t) - \theta_j(t)]$$

phases $\theta_i(t)$ in-degrees k_i

Kuramoto oscillator model (1975)

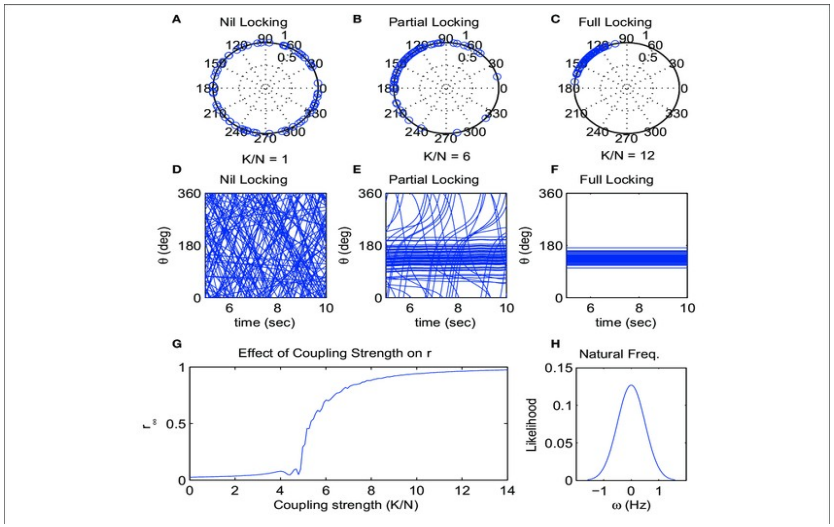

$$\dot{\theta}_i(t) = \omega_{i,0} + \frac{K}{k_i} \sum_j W_{ij} \sin[\theta_i(t) - \theta_j(t)]$$

phases $\theta_i(t)$ in-degrees k_i

global coupling K is the control parameter

Kuramoto oscillator model (1975)

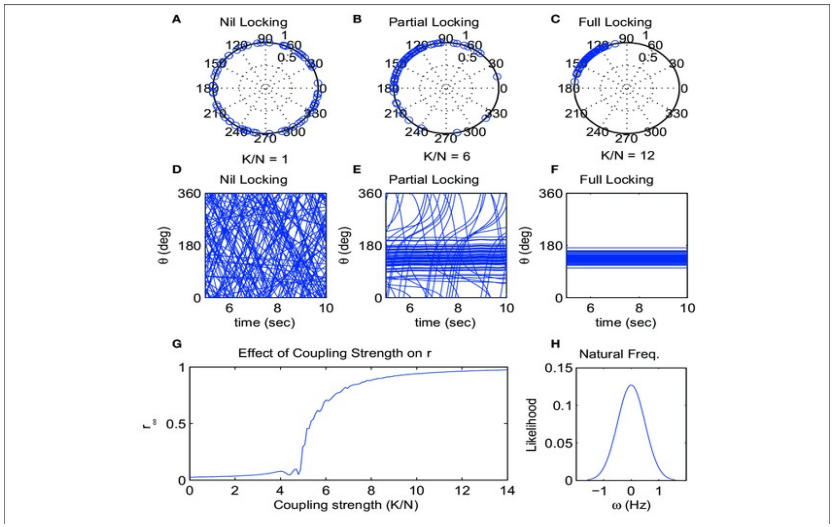

$$\dot{\theta}_i(t) = \omega_{i,0} + \frac{K}{k_i} \sum_j W_{ij} \sin[\theta_i(t) - \theta_j(t)]$$

phases $\theta_i(t)$ in-degrees k_i

global coupling K is the control parameter

weighted adjacency matrix W_{ij}

Kuramoto oscillator model (1975)

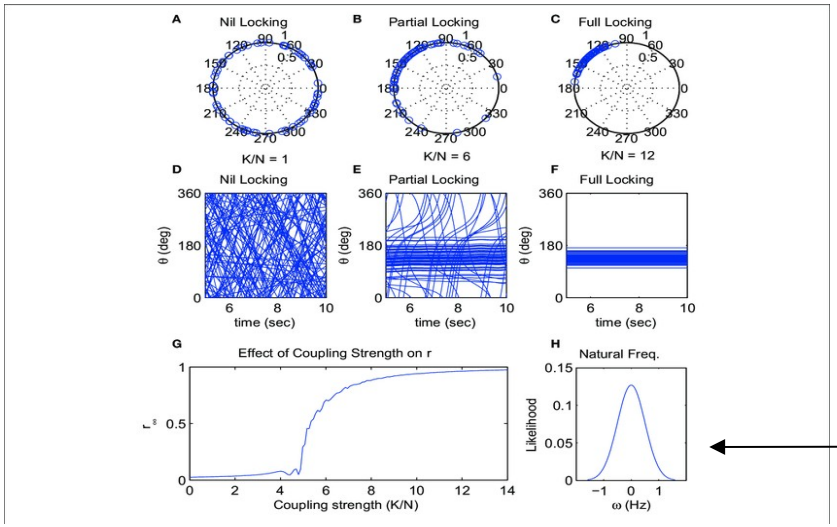

$$\dot{\theta}_i(t) = \omega_{i,0} + \frac{K}{k_i} \sum_j W_{ij} \sin[\theta_i(t) - \theta_j(t)]$$

phases $\theta_i(t)$ in-degrees k_i

global coupling K is the control parameter

weighted adjacency matrix W_{ij}

$\omega_{i,0}$ is the intrinsic frequency of the i-th oscillator,

Kuramoto oscillator model (1975)

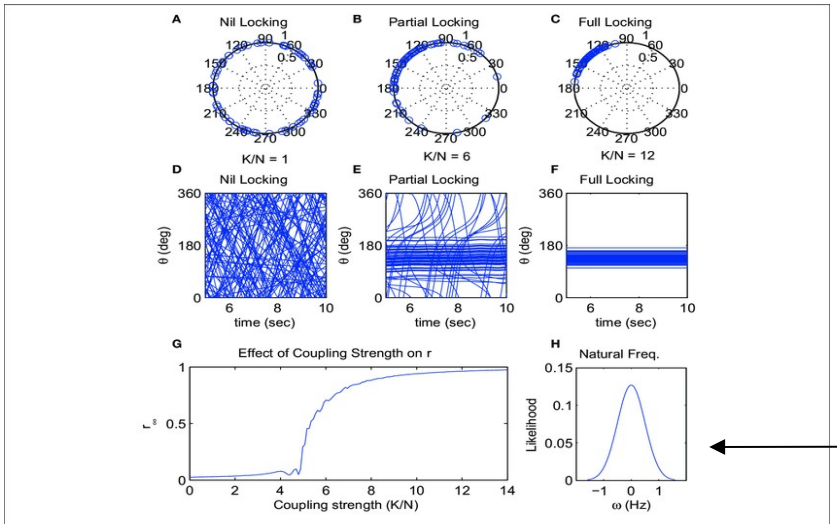

$$\dot{\theta}_i(t) = \omega_{i,0} + \frac{K}{k_i} \sum_j W_{ij} \sin[\theta_i(t) - \theta_j(t)]$$

phases $\theta_i(t)$ in-degrees k_i

global coupling K is the control parameter

weighted adjacency matrix W_{ij}

$\omega_{i,0}$ is the intrinsic frequency of the i-th oscillator,

$$R(t) = \frac{1}{N} \left| \sum_{j=1}^{N} e^{i\theta_j(t)} \right|$$

Order parameter : average phase:

Kuramoto oscillator model (1975)

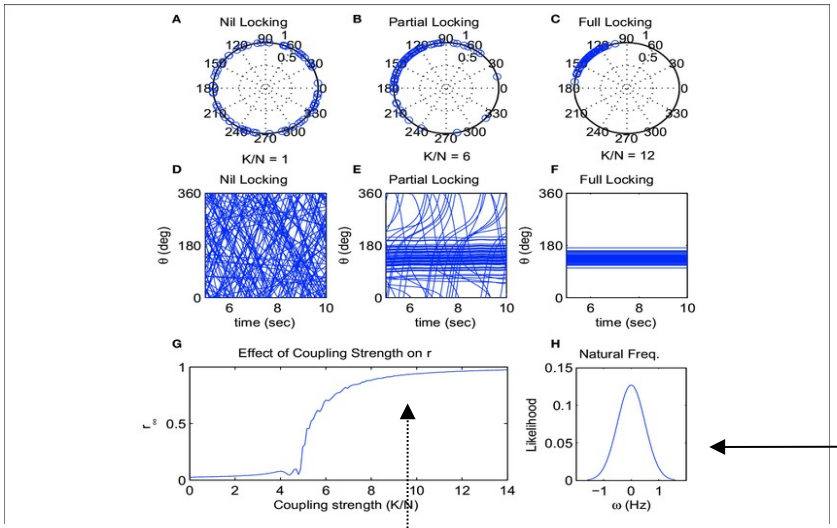

$$\dot{\theta}_i(t) = \omega_{i,0} + \frac{K}{k_i} \sum_j W_{ij} \sin[\theta_i(t) - \theta_j(t)]$$

phases $\theta_i(t)$ in-degrees k_i

global coupling K is the control parameter

weighted adjacency matrix W_{ij}

$\omega_{i,0}$ is the intrinsic frequency of the i-th oscillator,

$$R(t) = \frac{1}{N} \left| \sum_{j=1}^{N} e^{i\theta_j(t)} \right|$$

Order parameter : average phase:

Non-zero, above critical coupling strength $K > K_c$, tends to zero for $K \leq K_c$ as $R \propto (1/N)^{1/2}$

or exhibits an initial growth: $R(t, N) = N^{-1/2} t^{\eta} f_{\uparrow}(t/N^{\tilde{z}})$ *for incoherent initial state*

Kuramoto oscillator model (1975)

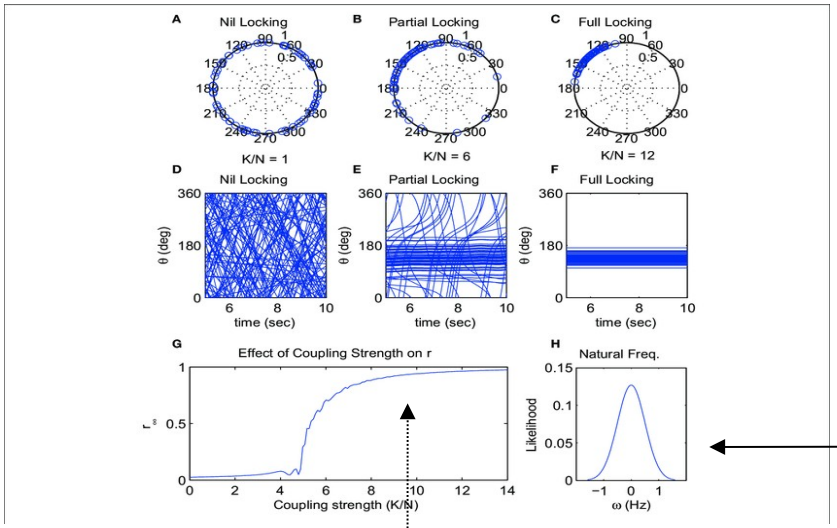

$$\dot{\theta}_i(t) = \omega_{i,0} + \frac{K}{k_i} \sum_j W_{ij} \sin[\theta_i(t) - \theta_j(t)]$$

phases $\theta_i(t)$ in-degrees k_i

global coupling K is the control parameter

weighted adjacency matrix W_{ij}

$\omega_{i,0}$ is the intrinsic frequency of the i-th oscillator,

$$R(t) = \frac{1}{N} \left| \sum_{j=1}^{N} e^{i\theta_j(t)} \right|$$

Order parameter : average phase:

Non-zero, above critical coupling strength $K > K_c$, tends to zero for $K \leq K_c$ as $R \propto (1/N)^{1/2}$

or exhibits an initial growth: $R(t, N) = N^{-1/2} t^{\eta} f_{\uparrow}(t/N^{\bar{z}})$ *for incoherent initial state*

Critical synchronization transition for D > 4 spatial dimensions

Kuramoto oscillator model (1975)

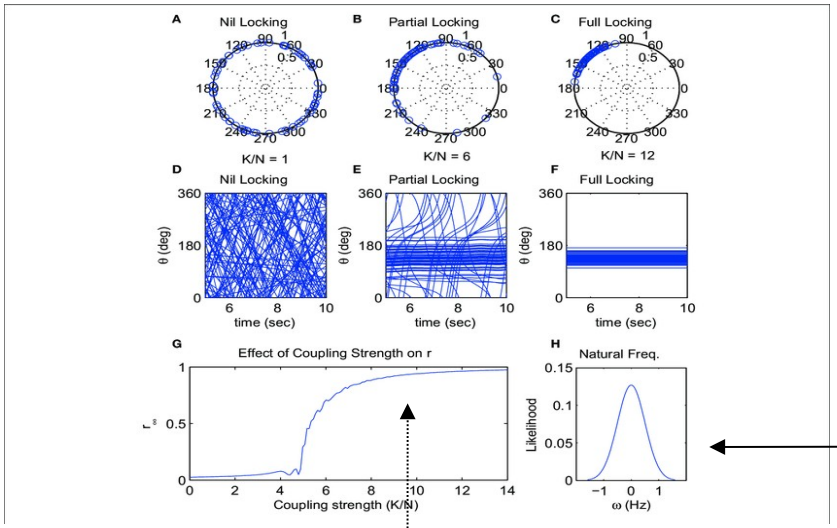

$$\dot{\theta}_i(t) = \omega_{i,0} + \frac{K}{k_i} \sum_j W_{ij} \sin[\theta_i(t) - \theta_j(t)]$$

phases $\theta_i(t)$ in-degrees k_i

global coupling K is the control parameter

weighted adjacency matrix W_{ij}

$\omega_{i,0}$ is the intrinsic frequency of the i-th oscillator,

$$R(t) = \frac{1}{N} \left| \sum_{j=1}^{N} e^{i\theta_j(t)} \right|$$

Order parameter : average phase:

Non-zero, above critical coupling strength $K > K_c$, tends to zero for $K \leq K_c$ as $R \propto (1/N)^{1/2}$
or exhibits an initial growth: $R(t, N) = N^{-1/2} t^{\eta} f_{\uparrow}(t/N^{\tilde{z}})$ *for incoherent initial state*

Critical synchronization transition for D > 4 spatial dimensions

The dynamical behavior suffers very strong corrections to scaling and chaoticity

We use this "toy" synchronization model assuming universality,

Kuramoto oscillator model (1975)

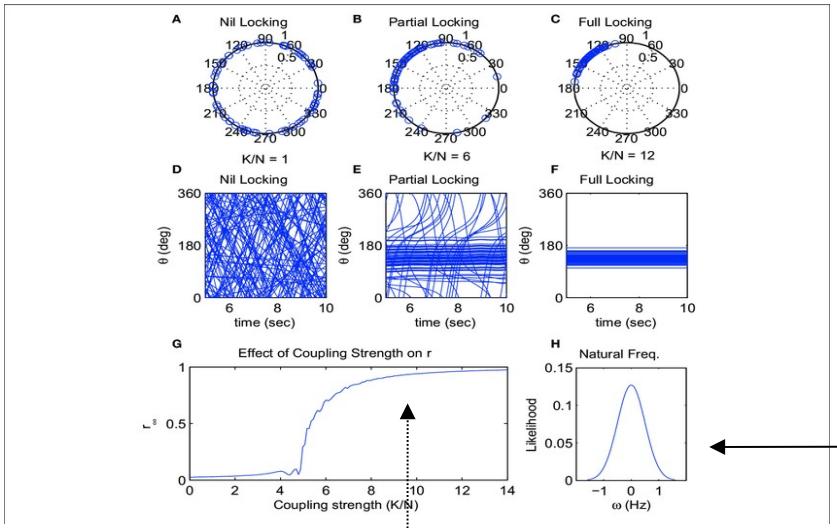

$$\dot{\theta}_i(t) = \omega_{i,0} + \frac{K}{k_i}\sum_j W_{ij}\sin[\theta_i(t) - \theta_j(t)]$$

phases $\theta_i(t)$ in-degrees k_i

global coupling K is the control parameter

weighted adjacency matrix W_{ij}

$\omega_{i,0}$ is the intrinsic frequency of the i-th oscillator,

$$R(t) = \frac{1}{N}\left|\sum_{j=1}^{N} e^{i\theta_j(t)}\right|$$

Order parameter : average phase:

Non-zero, above critical coupling strength $K > K_c$, tends to zero for $K \leq K_c$ as $R \propto (1/N)^{1/2}$
or exhibits an initial growth: $R(t,N) = N^{-1/2} t^{\eta} f_{\uparrow}(t/N^{\tilde{z}})$ *for incoherent initial state*

Critical synchronization transition for D > 4 spatial dimensions

The dynamical behavior suffers very strong corrections to scaling and chaoticity

We use this "toy" synchronization model assuming universality,
by solving the couple set of non-linear differential equations

HUN REN

Kuramoto oscillator model (1975)

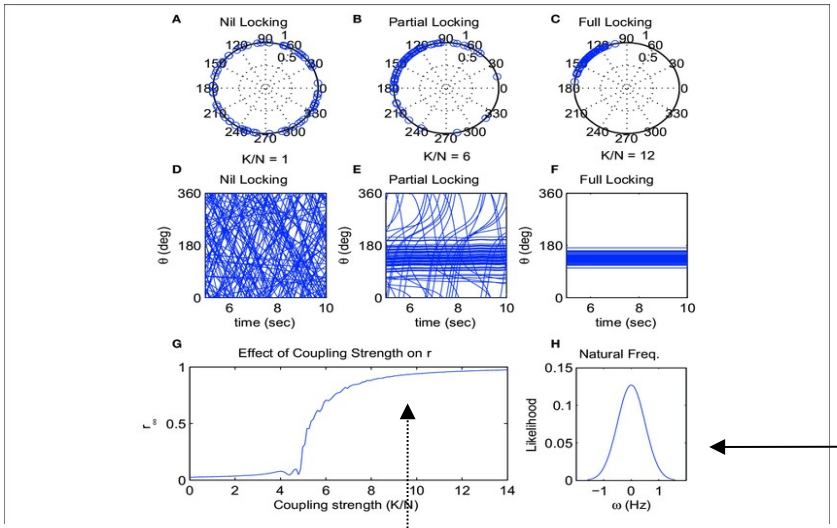

$$\dot{\theta}_i(t) = \omega_{i,0} + \frac{K}{k_i}\sum_j W_{ij}\sin[\theta_i(t) - \theta_j(t)]$$

phases $\theta_i(t)$ in-degrees k_i

global coupling K is the control parameter

weighted adjacency matrix W_{ij}

$\omega_{i,0}$ is the intrinsic frequency of the i-th oscillator,

Order parameter : average phase: $$R(t) = \frac{1}{N}\left|\sum_{j=1}^{N} e^{i\theta_j(t)}\right|$$

Non-zero, above critical coupling strength $K > K_c$, tends to zero for $K \leq K_c$ as $R \propto (1/N)^{1/2}$
or exhibits an initial growth: $R(t,N) = N^{-1/2}t^{\eta}f_{\uparrow}(t/N^{\tilde{z}})$ *for incoherent initial state*

Critical synchronization transition for D > 4 spatial dimensions

The dynamical behavior suffers very strong corrections to scaling and chaoticity

We use this "toy" synchronization model assuming universality,
by solving the couple set of non-linear differential equations
i.e. for ~100K nodes and millions of edges and for thousands of realizations, corresponding to different self frequencies
Vexcl and Boost CuDA libraries allowing 100x speedup with resp. CPUs

HUN REN

Numerical integration of the model

Numerical integration of the model

Global synchronization measures:

Numerical integration of the model

Global synchronization measures:

$$r(t)\exp i\theta(t) = 1/N\sum_j \exp\left[i\theta_j(t)\right]$$

Numerical integration of the model

Global synchronization measures:

$$r(t)\exp i\theta(t) = 1/N\sum_j \exp\left[i\theta_j(t)\right]$$

$$R(t) = \langle r(t)\rangle$$

Numerical integration of the model

Global synchronization measures:

$$r(t)\exp i\theta(t) = 1/N\sum_j \exp\left[i\theta_j(t)\right]$$

$$R(t) = \langle r(t)\rangle$$

$$\Omega(t) = \frac{1}{N}\sum_{j=1}^{N}(\overline{\omega}(t) - \omega_j^2(t))$$

Numerical integration of the model

Global synchronization measures:

$$r(t)\exp i\theta(t) = 1/N\sum_j \exp\left[i\theta_j(t)\right]$$

$$R(t) = \langle r(t)\rangle$$

$$\Omega(t) = \frac{1}{N}\sum_{j=1}^{N}(\overline{\omega}(t) - \omega_j^2(t))$$

Local synchronization measures:

Numerical integration of the model

Global synchronization measures:

$$r(t)\exp i\theta(t) = 1/N\sum_j \exp\left[i\theta_j(t)\right]$$

$$R(t) = \langle r(t)\rangle$$

$$\Omega(t) = \frac{1}{N}\sum_{j=1}^{N}(\overline{\omega}(t) - \omega_j^2(t))$$

Local synchronization measures:

$$R_i(t) = \frac{1}{N_{\text{i.neigh}}}\left|\sum_j^{N_{\text{i.neigh}}} A_{ij}e^{i\theta_j(t)}\right|$$

Numerical integration of the model

Global synchronization measures:

$$r(t)\exp i\theta(t) = 1/N\sum_j \exp\left[i\theta_j(t)\right]$$

$$R(t) = \langle r(t)\rangle \qquad \Omega(t) = \frac{1}{N}\sum_{j=1}^{N}(\overline{\omega}(t) - \omega_j^2(t))$$

Local synchronization measures:

$$R_i(t) = \frac{1}{N_{\text{i.neigh}}}\left|\sum_j^{N_{\text{i.neigh}}} A_{ij}e^{i\theta_j(t)}\right| \qquad \Omega_i(t) = \frac{1}{N_{\text{i.neigh}}}\left|\sum_j^{N_{\text{i.neigh}}} (\overline{\omega}(t) - \omega_j(t))^2\right|$$

Numerical integration of the model

Global synchronization measures:

$$r(t)\exp i\theta(t) = 1/N\sum_j \exp\left[i\theta_j(t)\right]$$

$$R(t) = \langle r(t)\rangle \qquad \Omega(t) = \frac{1}{N}\sum_{j=1}^{N}(\overline{\omega}(t) - \omega_j^2(t))$$

Local synchronization measures:

$$R_i(t) = \frac{1}{N_{\text{i.neigh}}}\left|\sum_j^{N_{\text{i.neigh}}} A_{ij}e^{i\theta_j(t)}\right| \qquad \Omega_i(t) = \frac{1}{N_{\text{i.neigh}}}\left|\sum_j^{N_{\text{i.neigh}}} (\overline{\omega}(t) - \omega_j(t))^2\right|$$

Hurst (phase) and beta (freq.) exponent analysis of local order parameters, to describe auto-correlations:

Numerical integration of the model

Global synchronization measures:

$$r(t)\exp i\theta(t) = 1/N\sum_j \exp\left[i\theta_j(t)\right]$$

$$R(t) = \langle r(t)\rangle \qquad \Omega(t) = \frac{1}{N}\sum_{j=1}^{N}(\overline{\omega}(t) - \omega_j^2(t))$$

Local synchronization measures:

$$R_i(t) = \frac{1}{N_{\text{i.neigh}}}\left|\sum_j^{N_{\text{i.neigh}}} A_{ij}e^{i\theta_j(t)}\right| \qquad \Omega_i(t) = \frac{1}{N_{\text{i.neigh}}}\left|\sum_j^{N_{\text{i.neigh}}} (\overline{\omega}(t) - \omega_j(t))^2\right|$$

Hurst (phase) and beta (freq.) exponent analysis of local order parameters, to describe auto-correlations:

$$\mathbb{E}\left[\frac{Z(n)}{S(n)}\right] = Cn^H$$

Numerical integration of the model

Global synchronization measures:

$$r(t)\exp i\theta(t) = 1/N\sum_j \exp\left[i\theta_j(t)\right]$$

$$R(t) = \langle r(t)\rangle \qquad \Omega(t) = \frac{1}{N}\sum_{j=1}^{N}(\overline{\omega}(t) - \omega_j^2(t))$$

Local synchronization measures:

$$R_i(t) = \frac{1}{N_{\text{i.neigh}}}\left|\sum_j^{N_{\text{i.neigh}}} A_{ij}e^{i\theta_j(t)}\right| \qquad \Omega_i(t) = \frac{1}{N_{\text{i.neigh}}}\left|\sum_j^{N_{\text{i.neigh}}}(\overline{\omega}(t) - \omega_j(t))^2\right|$$

Hurst (phase) and beta (freq.) exponent analysis of local order parameters, to describe auto-correlations:

$$\mathbb{E}\left[\frac{Z(n)}{S(n)}\right] = Cn^H \qquad S(f) = \left|\sum_{j=0}^{N}\Omega_j(t)e^{-2\pi i f_j/N}\right|^2 \approx 1/f^\beta$$

Numerical integration of the model

Global synchronization measures:

$$r(t)\exp i\theta(t) = 1/N\sum_j \exp\left[i\theta_j(t)\right]$$

$$R(t) = \langle r(t)\rangle \qquad \Omega(t) = \frac{1}{N}\sum_{j=1}^{N}(\overline{\omega}(t) - \omega_j^2(t))$$

Local synchronization measures:

$$R_i(t) = \frac{1}{N_{\text{i.neigh}}}\left|\sum_j^{N_{\text{i.neigh}}} A_{ij}e^{i\theta_j(t)}\right| \qquad \Omega_i(t) = \frac{1}{N_{\text{i.neigh}}}\left|\sum_j^{N_{\text{i.neigh}}}(\overline{\omega}(t) - \omega_j(t))^2\right|$$

Hurst (phase) and beta (freq.) exponent analysis of local order parameters, to describe auto-correlations:

$$\mathbb{E}\left[\frac{Z(n)}{S(n)}\right] = Cn^H \qquad S(f) = \left|\sum_{j=0}^{N}\Omega_j(t)e^{-2\pi i f_j/N}\right|^2 \approx 1/f^\beta$$

Numerical ODE solution of large set of equations via adaptive

Bulrisch-Stoer stepper, implemented on HPC GPU-s

HUN REN

Fruit-fly connecome synchronization results

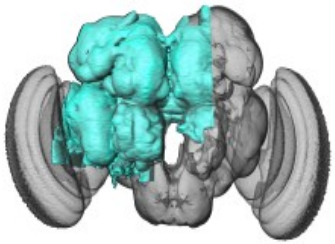

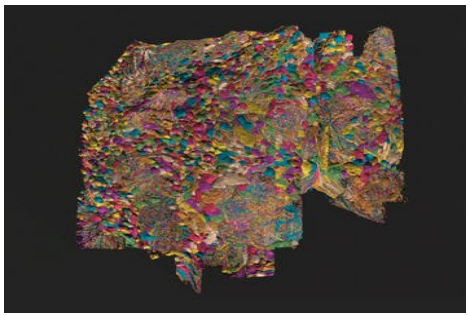

A_{ij}

G.O, G.D, J.K Phys. Rev. Res. 4 (2022) 023057.

Fruit-fly connecome synchronization results

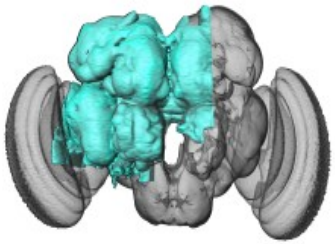

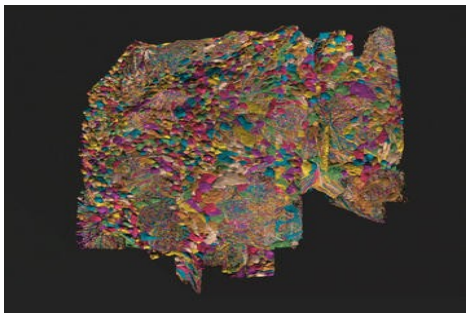

A_{ij}

Fruit-fly connectome is the largest exactly known neural network:

$N = 21.615, L = 3.410.247$

G.O, G.D, J.K Phys. Rev. Res. 4 (2022) 023057.

Fruit-fly connecome synchronization results

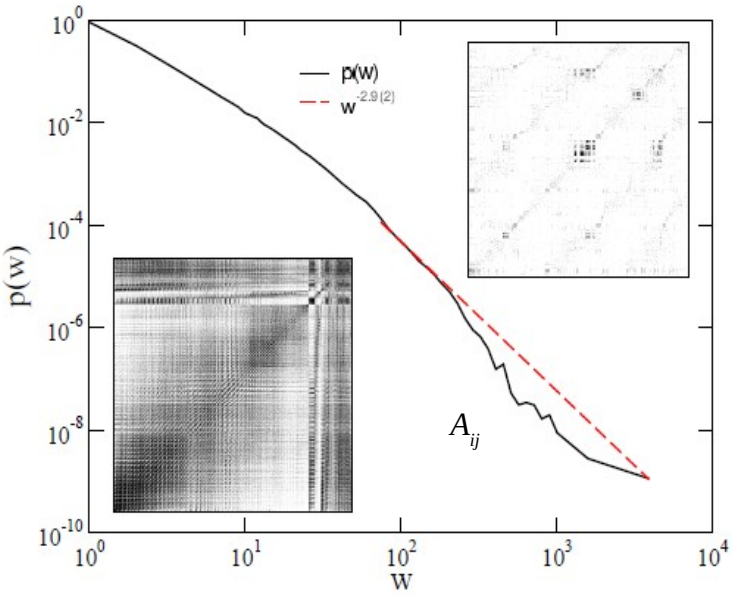

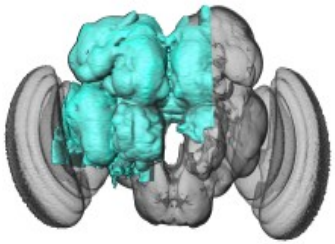

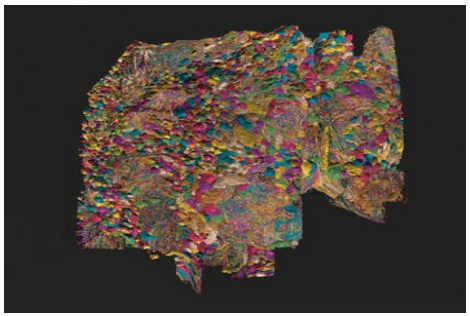

Fruit-fly connectome is the largest exactly known neural network:

$N = 21.615, L = 3.410.247$

Similar to random Erdős-Rényi (ER) graph, but power-law tailed connection weights

G.O, G.D, J.K Phys. Rev. Res. 4 (2022) 023057.

Fruit-fly connecome synchronization results

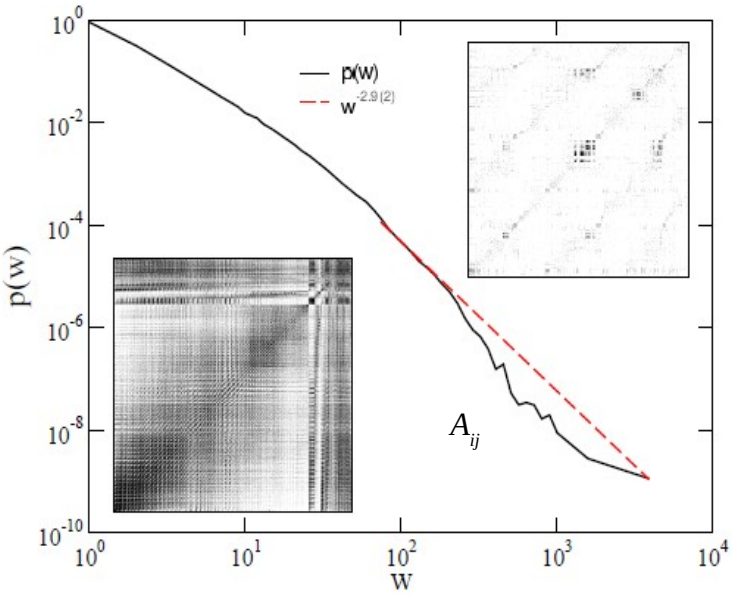

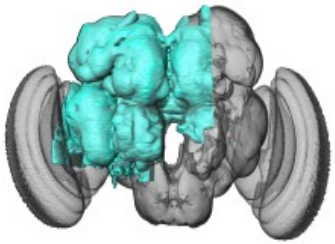

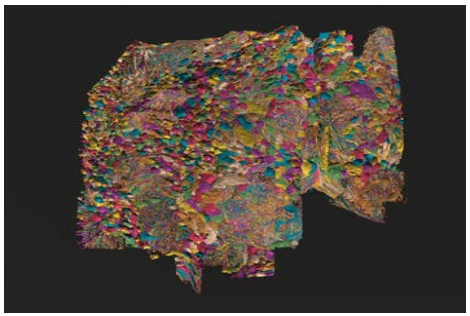

Fruit-fly connectome is the largest exactly known neural network:

$N = 21.615, L = 3.410.247$

Similar to random Erdős-Rényi (ER) graph, but power-law tailed connection weights
Weakly modular

G.O, G.D, J.K Phys. Rev. Res. 4 (2022) 023057.

Fruit-fly connecome synchronization results

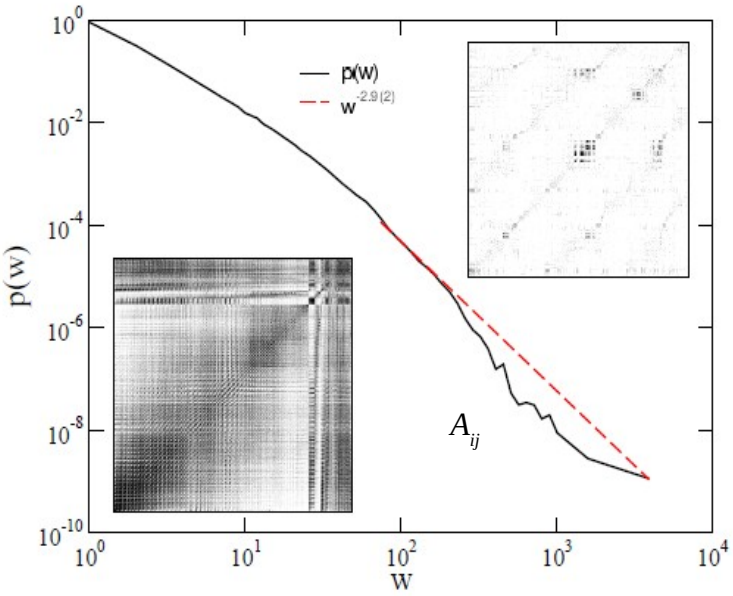

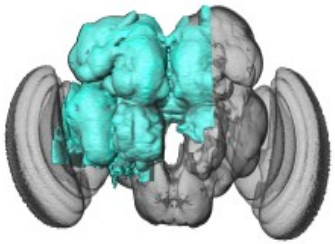

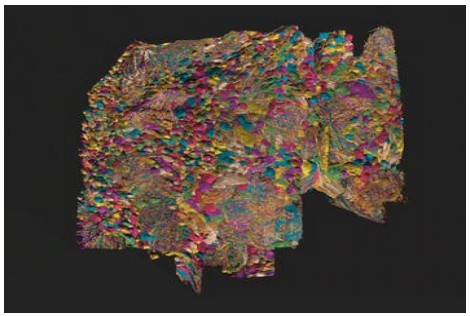

Fruit-fly connectome is the largest exactly known neural network:

$N = 21.615, L = 3.410.247$

Similar to random Erdős-Rényi (ER) graph, but power-law tailed connection weights
Weakly modular

Synchronziation transition via *R(t)*
local slopes : $\eta = -d\ lnR\ /\ d\ lnt$

G.O, G.D, J.K Phys. Rev. Res. 4 (2022) 023057.

HUN REN

Fruit-fly connecome synchronization results

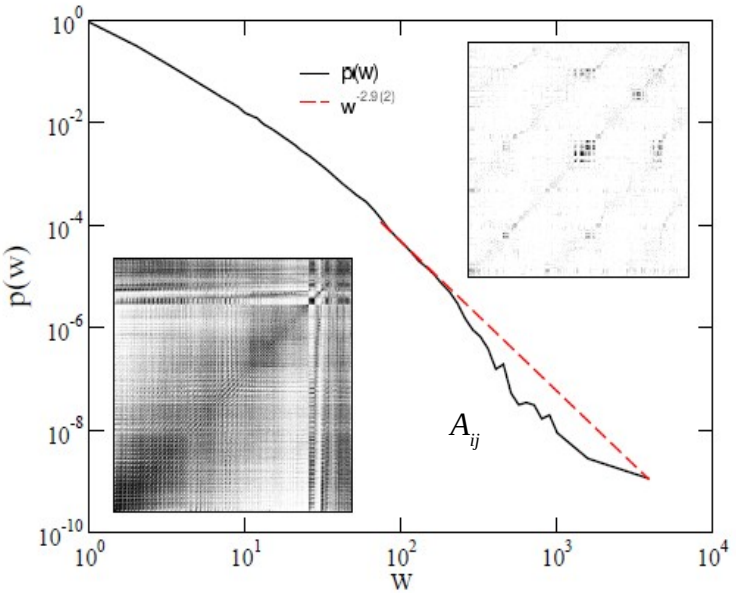

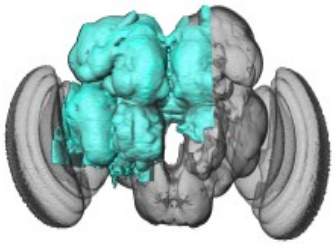

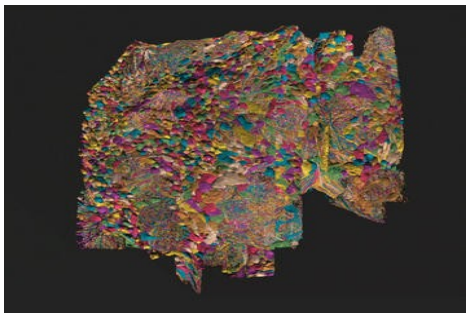

Fruit-fly connectome is the largest exactly known neural network:

$N = 21.615, L = 3.410.247$

Similar to random Erdős-Rényi (ER) graph, but power-law tailed connection weights
Weakly modular

Synchronziation transition via *R(t)*
local slopes : $\eta = -d\ lnR\ /\ d\ lnt$

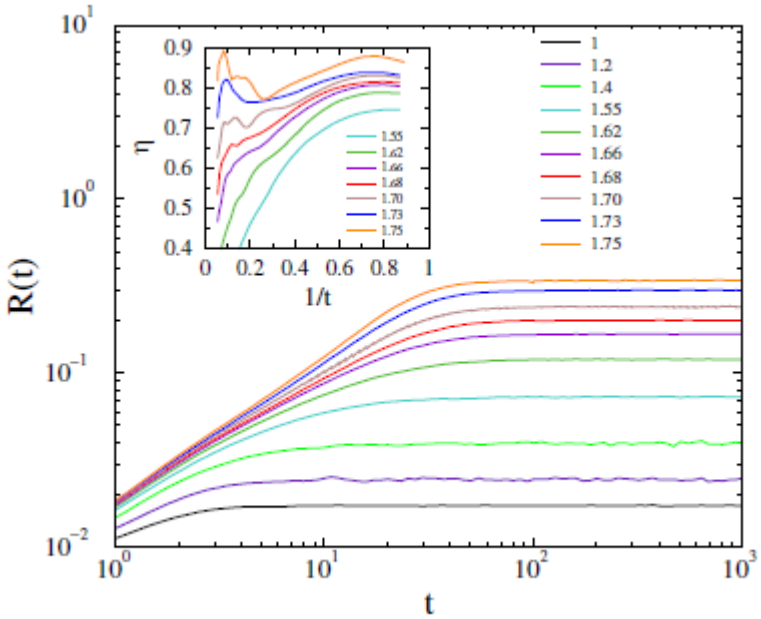

G.O, G.D, J.K Phys. Rev. Res. 4 (2022) 023057.

HUN REN

Fruit-fly connecome synchronization results

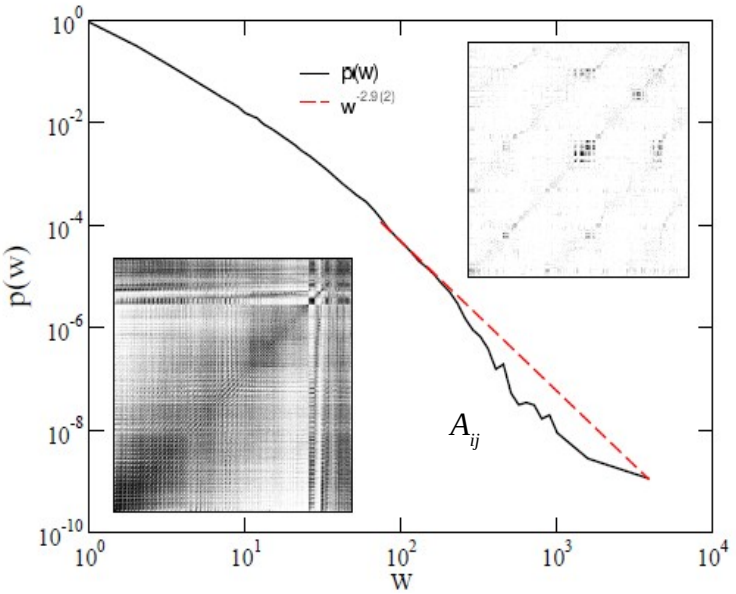

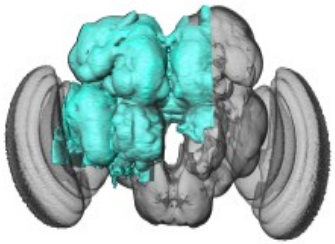

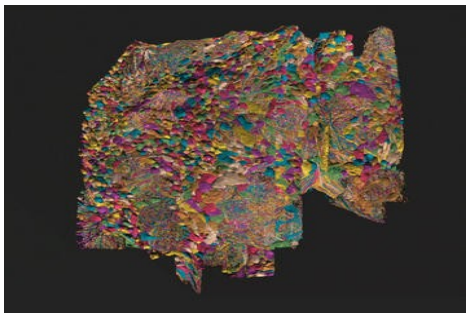

Fruit-fly connectome is the largest exactly known neural network:

$N = 21.615, L = 3.410.247$

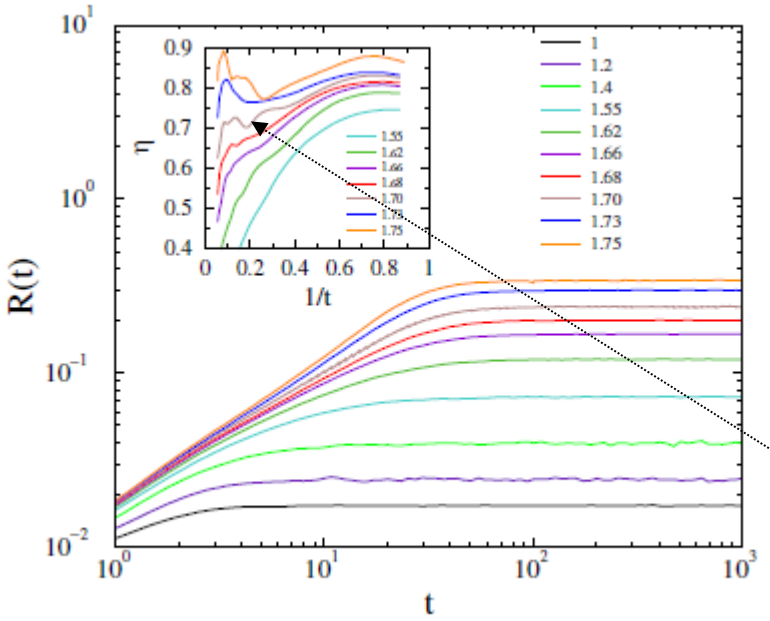

Similar to random Erdős-Rényi (ER) graph, but power-law tailed connection weights
Weakly modular

Synchronziation transition via *R(t)*
local slopes : $\eta = -d\ lnR / d\ lnt$

$K_c = 1.60(1)$ (inflexion curve)
Characterized by the growth exponent $\eta = 0.7(1)$

G.O, G.D, J.K Phys. Rev. Res. 4 (2022) 023057.

HUN REN

Synchronization transitions on connectome graphs with periodic external force (task state)

Synchronization transitions on connectome graphs with periodic external force (task state)

Shinomoto-Kuramoto oscillator model synchronization transition:

θ_i: angle, K: global coupling

Synchronization transitions on connectome graphs with periodic external force (task state)

Shinomoto-Kuramoto oscillator model synchronization transition:

$$\dot{\theta}_j(t) = \omega_j^0 + K \sum_k W_{jk} \sin[\theta_k(t) - \theta_j(t)] + F \sin(\theta_j(t)) + \epsilon \eta_j(t) \ .$$

θ_i: angle, K: global coupling

F: external force, η_i: noise

Synchronization transitions on connectome graphs with periodic external force (task state)

Shinomoto-Kuramoto oscillator model synchronization transition:

$$\dot{\theta}_j(t) = \omega_j^0 + K \sum_k W_{jk} \sin[\theta_k(t) - \theta_j(t)] + F \sin(\theta_j(t)) + \epsilon \eta_j(t) \ .$$

θ_i: angle, K: global coupling

F: external force, η_i: noise

Quenched heterogeneity in self-frequencies and network topology

Synchronization transitions on connectome graphs with periodic external force (task state)

Shinomoto-Kuramoto oscillator model synchronization transition:

$$\dot{\theta}_j(t) = \omega_j^0 + K \sum_k W_{jk} \sin[\theta_k(t) - \theta_j(t)] + F \sin(\theta_j(t)) + \epsilon \eta_j(t) \ .$$

θ_i: angle, K: global coupling

F: external force, η_i: noise

Quenched heterogeneity in self-frequencies and network topology

Synchronization transitions on connectome graphs with periodic external force (task state)

Shinomoto-Kuramoto oscillator model synchronization transition:

$$\dot{\theta}_j(t) = \omega_j^0 + K \sum_k W_{jk} \sin[\theta_k(t) - \theta_j(t)] + F \sin(\theta_j(t)) + \epsilon \eta_j(t) \ .$$

θ_i: angle, K: global coupling

F: external force, η_i: noise

Quenched heterogeneity in self-frequencies and network topology

$R_i(t)$

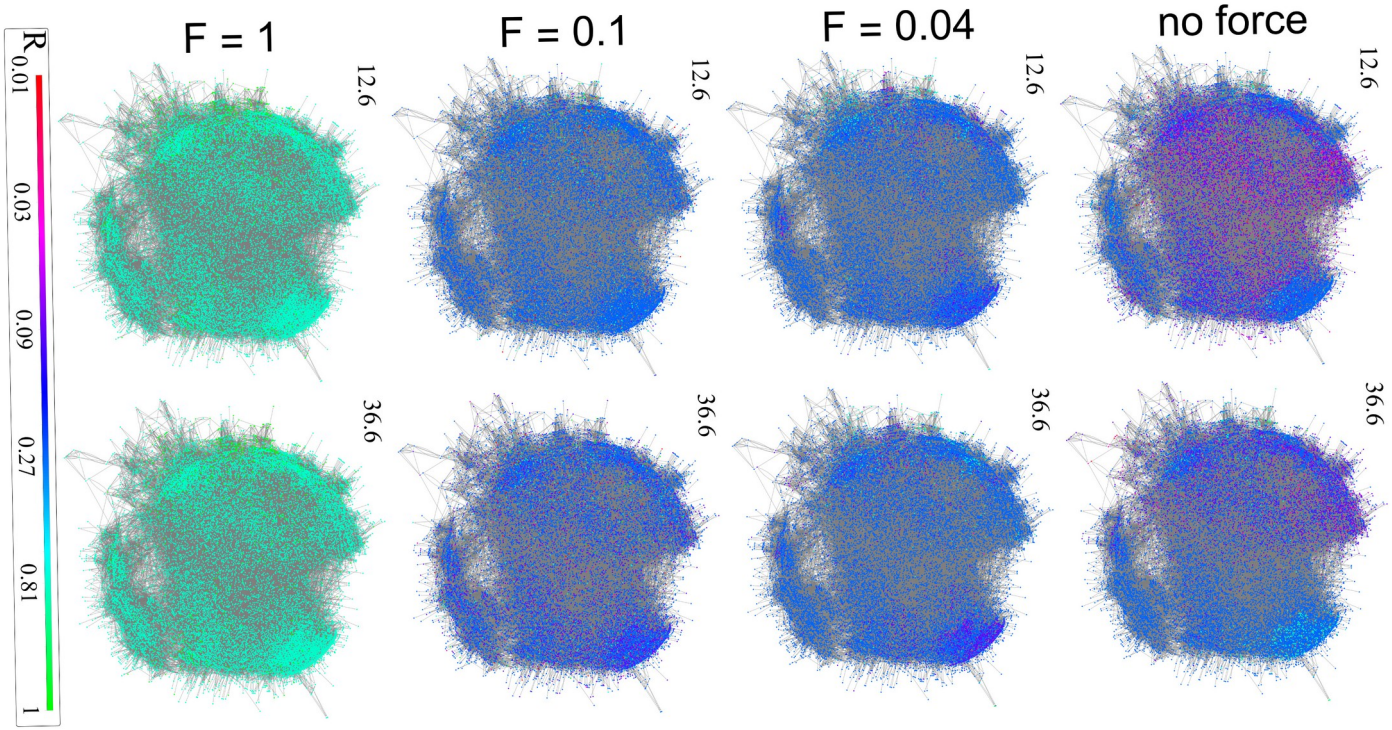

HUN REN

Force induced synchronization

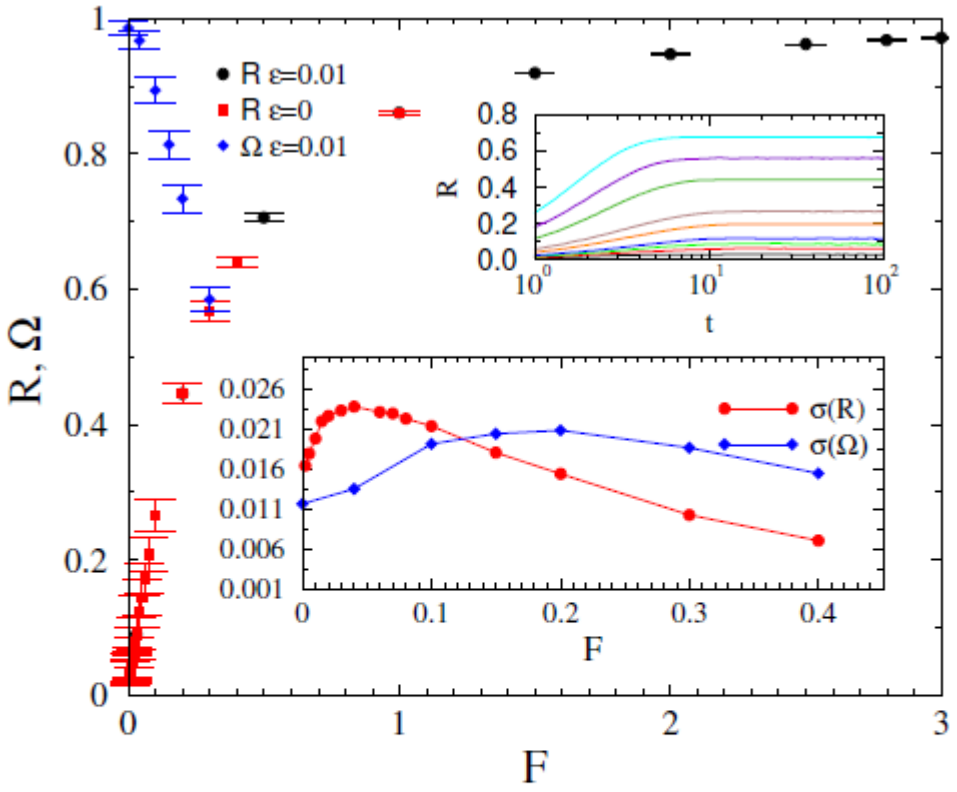

FIG. 1: Order parameter dependence on F for the fruit-fly connectome for the noisy (black bullet) and the noiseless (red boxes) cases at $K = 1.3$. The blue diamonds show the steady-state Ω values with noise. Lower inset: Variances of R and Ω for the noisy case. Upper inset: Time dependence of the noisy $R(t)$, for $F = 0, 0.02, 0.03, 0.04, 0.07, 0.1, 0.2, 0.3, 0.4$ (bottom to top curves).

Force induced synchronization

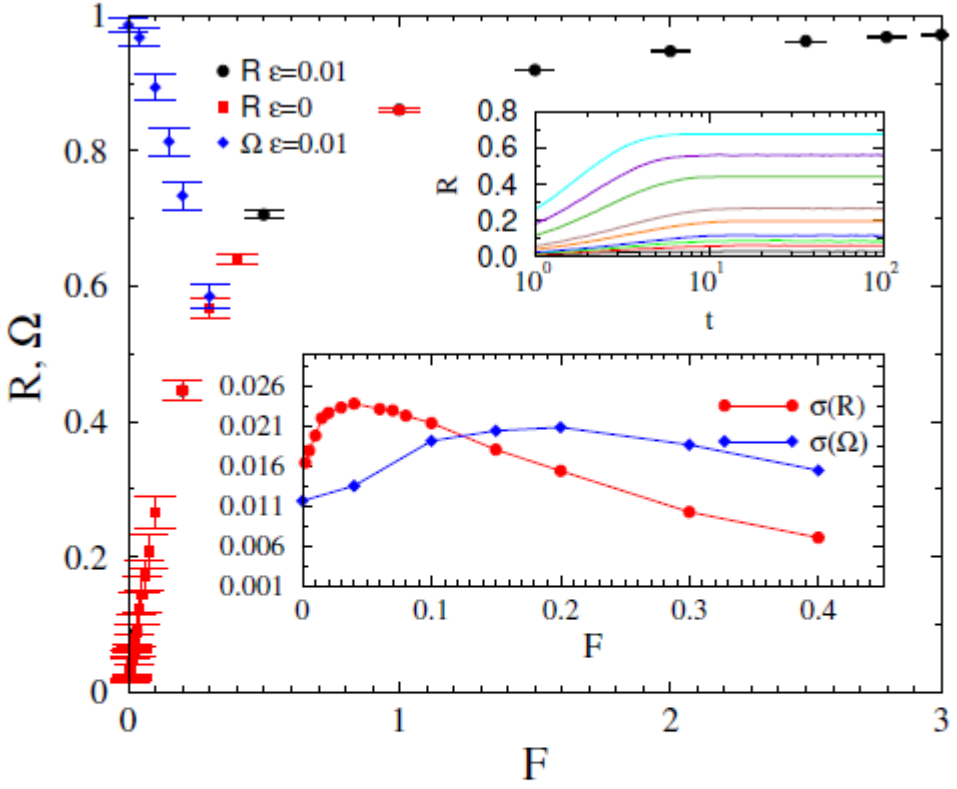

FIG. 1: Order parameter dependence on F for the fruit-fly connectome for the noisy (black bullet) and the noiseless (red boxes) cases at $K = 1.3$. The blue diamonds show the steady-state Ω values with noise. Lower inset: Variances of R and Ω for the noisy case. Upper inset: Time dependence of the noisy $R(t)$, for $F = 0$, 0.02, 0.03, 0.04, 0.07, 0.1, 0.2, 0.3, 0.4 (bottom to top curves).

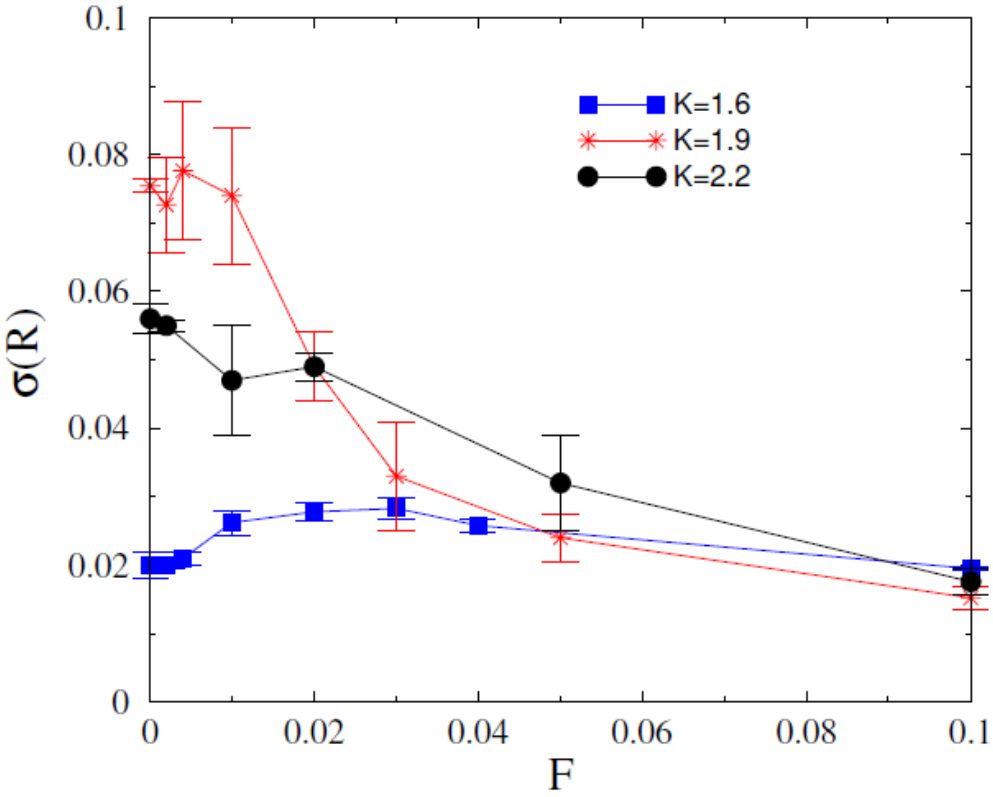

Dependence of the steady state SK order parameter ® on the global coupling K and on the force F. One can observe a maximum at *K ~1.9* and *F = 0* (case (w)), i.e at synchronization transition of the resting state of the brain.

Hurst and beta exponent analysis for the fly and human brain nets

Hurst and beta exponent analysis for the fly and human brain nets

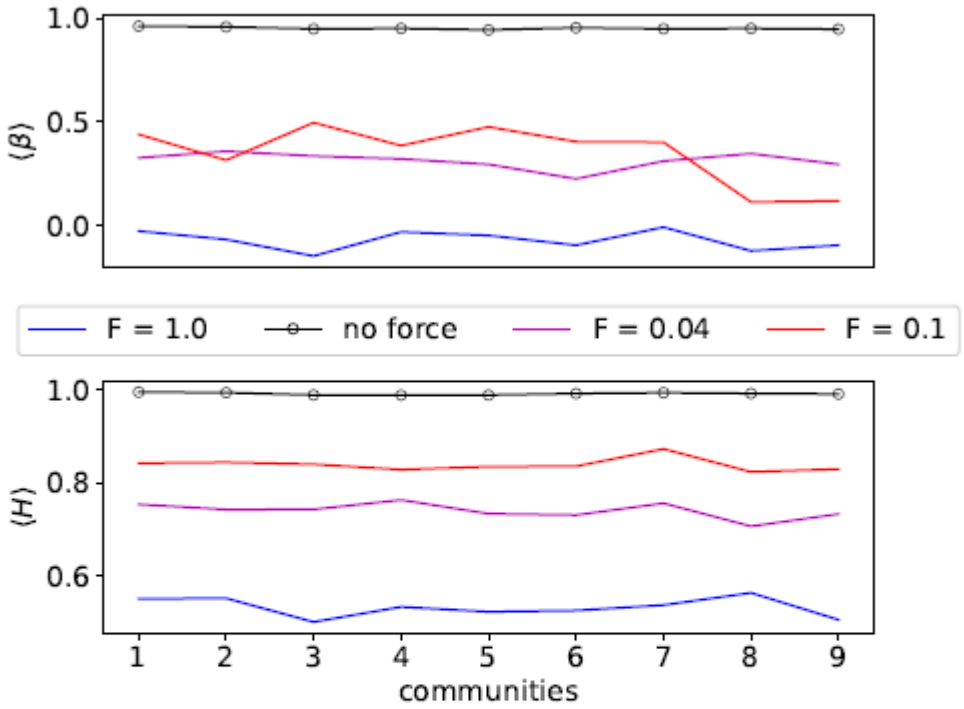

FIG. 8: Hurst and beta exponents of all fruit-fly connectome communities. In the forceless case at the critical Hopf transition coupling, the H exponent is the largest for every community. With forces these values drop for each community. This shows a resemblance with the rest and non-rest studies of different brain areas in [63], showing $\langle H \rangle \approx 1.0$ at resting state and $\langle H \rangle \approx 0.7$ at task driven states.

Hurst and beta exponent analysis for the fly and human brain nets

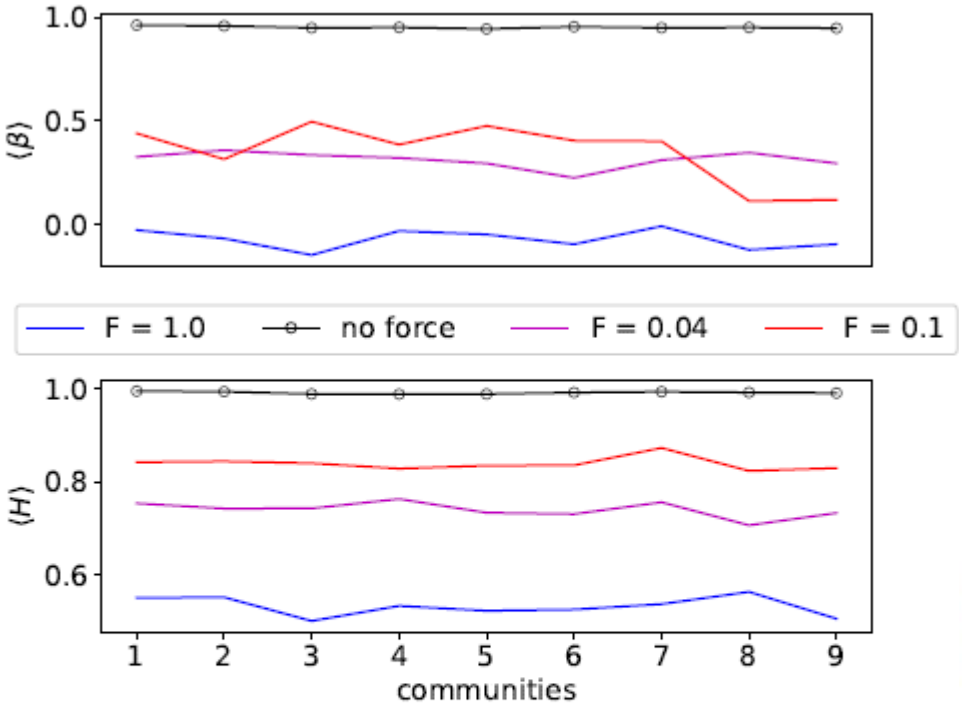

FIG. 8: Hurst and beta exponents of all fruit-fly connectome communities. In the forceless case at the critical Hopf transition coupling, the H exponent is the largest for every community. With forces these values drop for each community. This shows a resemblance with the rest and non-rest studies of different brain areas in [63], showing $\langle H \rangle \approx 1.0$ at resting state and $\langle H \rangle \approx 0.7$ at task driven states.

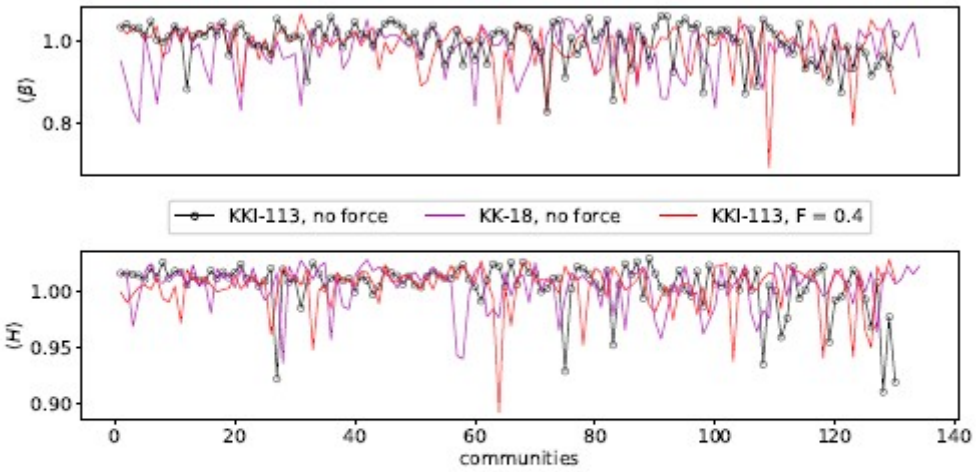

FIG. 9: Hurst and β exponents of all human connectomes' communities. KKI-113 is presented with and without force terms and KK-18 without the force terms.

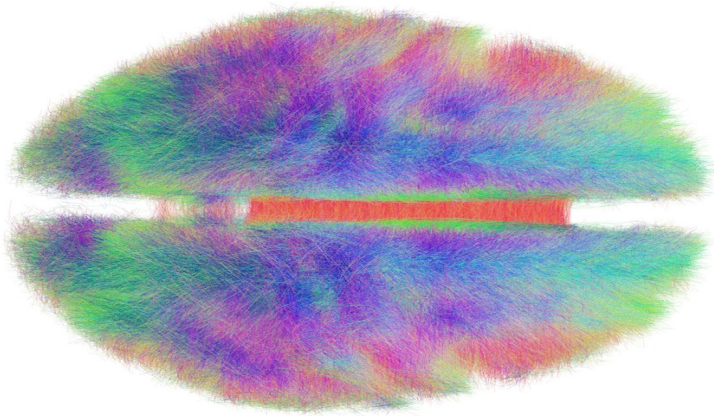

FMRI experiments

Community dependent synch.

Quasi-criticality, like in fMRI experiments: *Ochab et al, Sci. Rep. 12, 17866 (2022).*

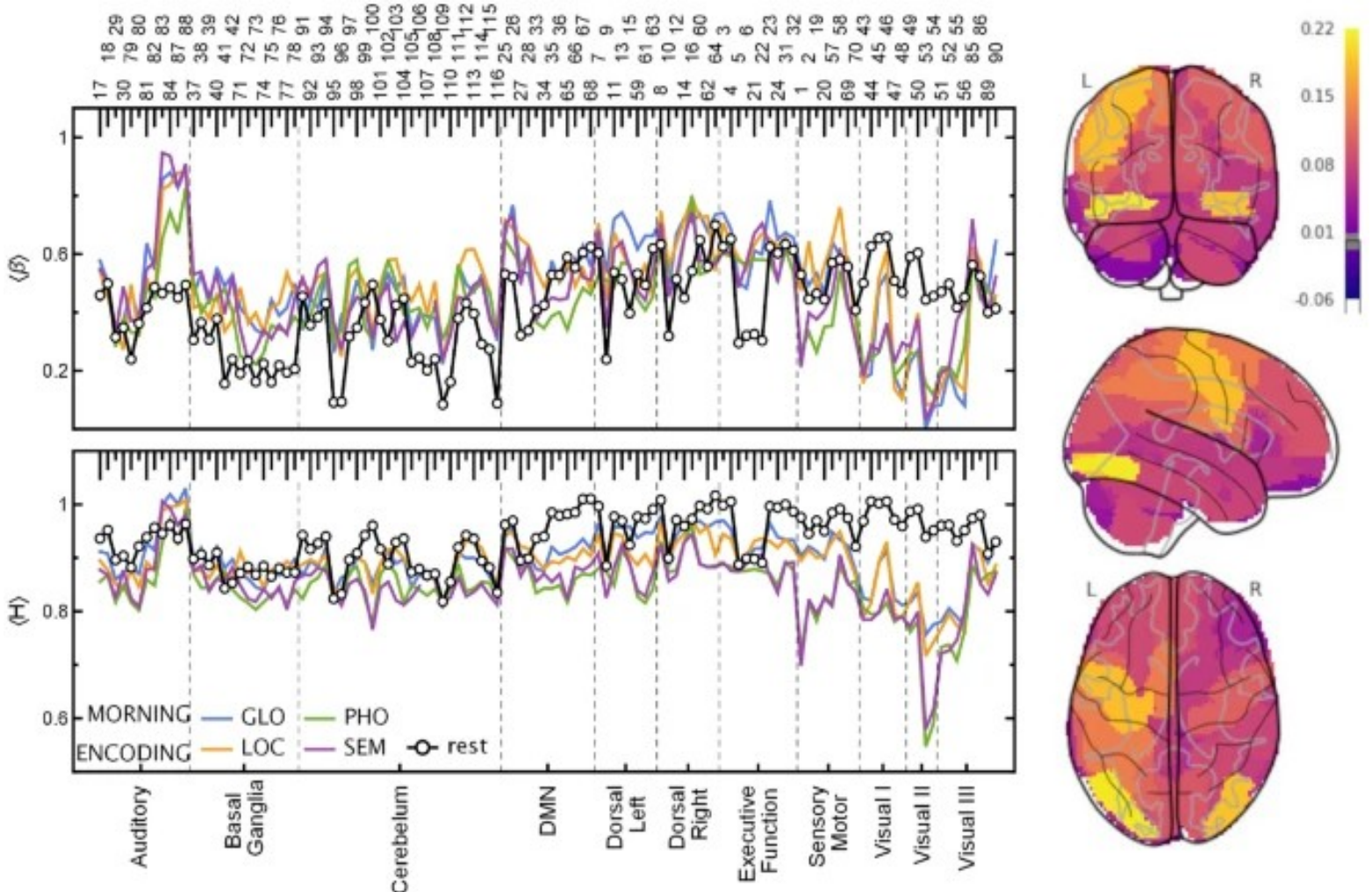

Task ↔ rest state operation

Violation of the fluctuation-dissipation theory versus interaction anisotropy

Characterizes distance from equilibrium, we tested at criticality

Violation of the fluctuation-dissipation theory versus interaction anisotropy

Characterizes distance from equilibrium, we tested at criticality

Auto-correlation: $A(t,s) = \langle E(t)E(s) \rangle$

Violation of the fluctuation-dissipation theory versus interaction anisotropy

Characterizes distance from equilibrium, we tested at criticality

Auto-correlation: $A(t,s) = \langle E(t)E(s)\rangle$ $A(t/s) \propto s^{-b}(t/s)^{-\lambda_A/Z}$

Violation of the fluctuation-dissipation theory versus interaction anisotropy

Characterizes distance from equilibrium, we tested at criticality

Auto-correlation: $A(t,s) = \langle E(t)E(s)\rangle$ $A(t/s) \propto s^{-b}(t/s)^{-\lambda_A/Z}$

Auto-response: $\mathcal{R}(t,s) = \frac{\delta E_h(t,s)}{\delta h}|_h \to 0$,

Violation of the fluctuation-dissipation theory versus interaction anisotropy

Characterizes distance from equilibrium, we tested at criticality

Auto-correlation: $A(t,s) = \langle E(t)E(s)\rangle$ $\qquad A(t/s) \propto s^{-b}(t/s)^{-\lambda_A/Z}$

Auto-response: $\mathcal{R}(t,s) = \frac{\delta E_h(t,s)}{\delta h}|_h \to 0\ ,$ $\qquad \mathcal{R}(t/s) \propto s^{-1-a}(t/s)^{-\lambda_\mathcal{R}/Z}$

Violation of the fluctuation-dissipation theory versus interaction anisotropy

Characterizes distance from equilibrium, we tested at criticality

Auto-correlation: $A(t,s) = \langle E(t)E(s)\rangle$ $\qquad A(t/s) \propto s^{-b}(t/s)^{-\lambda_A/Z}$

Auto-response: $\mathcal{R}(t,s) = \frac{\delta E_h(t,s)}{\delta h}|_h \to 0\ ,$ $\qquad \mathcal{R}(t/s) \propto s^{-1-a}(t/s)^{-\lambda_\mathcal{R}/Z}$

X(t,s): violation: $\mathcal{R}(t,s) = \frac{1}{T}X(t,s)\frac{\partial A(t,s)}{\partial s}$

Violation of the fluctuation-dissipation theory versus interaction anisotropy

Characterizes distance from equilibrium, we tested at criticality

Auto-correlation: $A(t,s) = \langle E(t)E(s)\rangle$ $\qquad A(t/s) \propto s^{-b}(t/s)^{-\lambda_A/Z}$

Auto-response: $\mathcal{R}(t,s) = \frac{\delta E_h(t,s)}{\delta h}|_h \to 0\ ,$ $\qquad \mathcal{R}(t/s) \propto s^{-1-a}(t/s)^{-\lambda_{\mathcal{R}}/Z}$

X(t,s): violation: $\mathcal{R}(t,s) = \frac{1}{T}X(t,s)\frac{\partial A(t,s)}{\partial s}$

Anisotropy in the weights in different brain states $\alpha = 1/N\sum_{i,j}^{N}(W_{ij} - W_{ji})$

Violation of the fluctuation-dissipation theory versus interaction anisotropy

Characterizes distance from equilibrium, we tested at criticality

Auto-correlation: $A(t,s) = \langle E(t)E(s) \rangle$ $\quad A(t/s) \propto s^{-b}(t/s)^{-\lambda_A/Z}$

Auto-response: $\mathcal{R}(t,s) = \frac{\delta E_h(t,s)}{\delta h}|_h \to 0\ ,$ $\quad \mathcal{R}(t/s) \propto s^{-1-a}(t/s)^{-\lambda_\mathcal{R}/Z}$

X(t,s): violation: $\mathcal{R}(t,s) = \frac{1}{T} X(t,s) \frac{\partial A(t,s)}{\partial s}$

Anisotropy in the weights in different brain states $\alpha = 1/N \sum_{i,j}^{N} (W_{ij} - W_{ji})$

Measured phase response: $R(t,s) = 1/N \sum_{i=1}^{N} \cos(\theta_i'(t) - \theta_i(t))$

HUN REN

Violation of the fluctuation-dissipation theory versus interaction anisotropy

Characterizes distance from equilibrium, we tested at criticality

Auto-correlation: $A(t,s) = \langle E(t)E(s)\rangle$ $\qquad A(t/s) \propto s^{-b}(t/s)^{-\lambda_A/Z}$

Auto-response: $\mathcal{R}(t,s) = \frac{\delta E_h(t,s)}{\delta h}|_h \to 0\ ,$ $\qquad \mathcal{R}(t/s) \propto s^{-1-a}(t/s)^{-\lambda_{\mathcal{R}}/Z}$

X(t,s): violation: $\mathcal{R}(t,s) = \frac{1}{T}X(t,s)\frac{\partial A(t,s)}{\partial s}$

Anisotropy in the weights in different brain states $\alpha = 1/N\sum_{i,j}^{N}(W_{ij} - W_{ji})$

Measured phase response: $R(t,s) = 1/N\sum_{i=1}^{N}\cos(\theta_i^{'}(t) - \theta_i(t))$

Measured phase correlator: $A(t,s) = 1/N\sum_{i=1}^{N}\cos(\theta_i(t) - \theta_i(s)])$

HUN REN

Phase auto-correlation results on the Fly connectome at the synchonization (critical) point

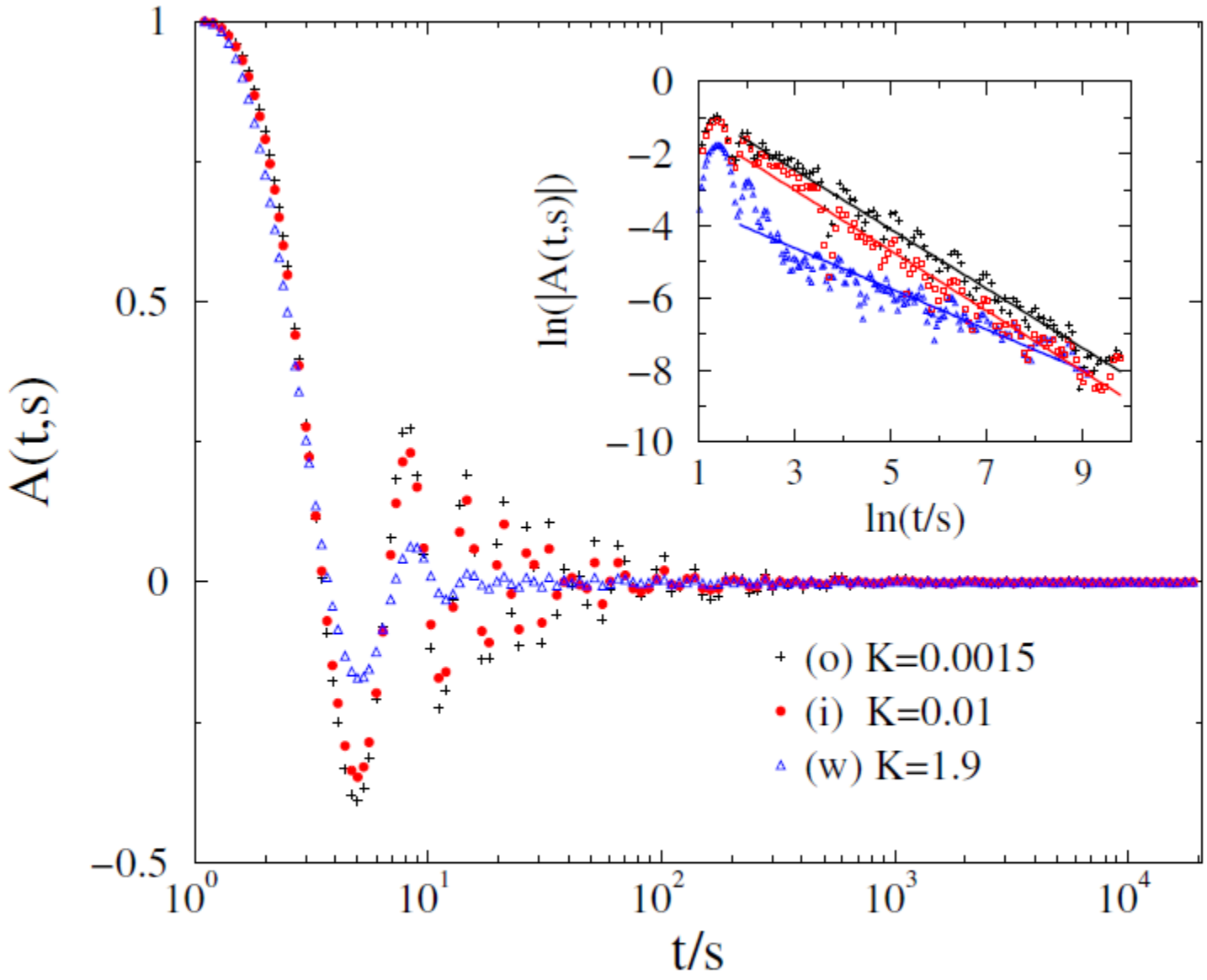

FIG. 8. Critical auto-correlation functions for $s = 1$ in the Kuramoto model, for different anisotropy scenarios labeled by the legends. Inset: Absolute value of the same on logarithmic scales. Dashed lines show PL fits for the tails.

Phase auto-respose results on the Fly connectome at the synchonization (critical) point

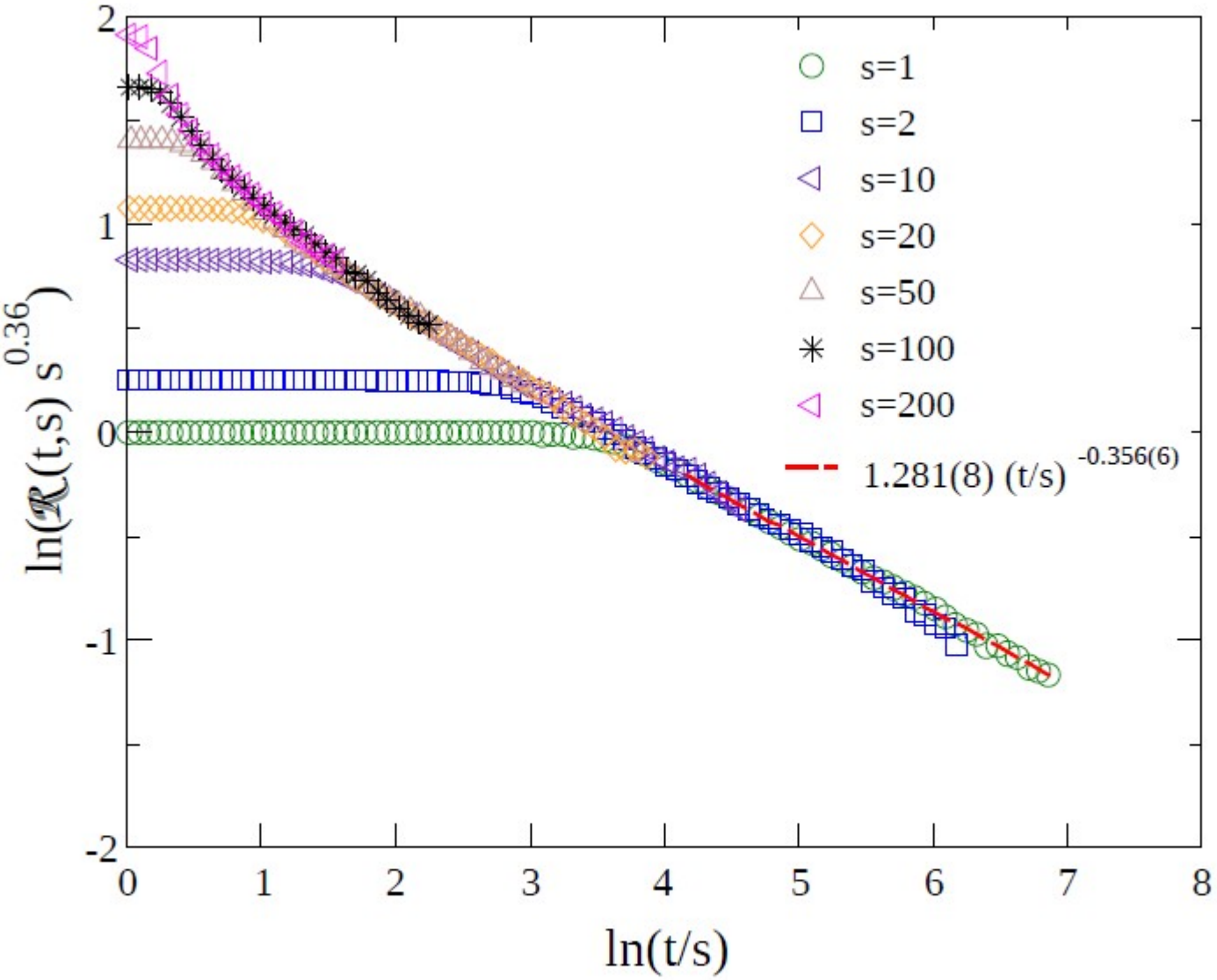

FIG. 11. Scaling collapse of the auto-responses $\mathcal{R}(t,s)_i$ in the Kuramoto model for different s values indicated by the lege in case of scenario (i) at the critical point: $K_c = 0.01$. The dashed line shows PL fitting for the tail: $\ln(t/s) > 4$.

vFD for different (o,i,w) anisotropy levels

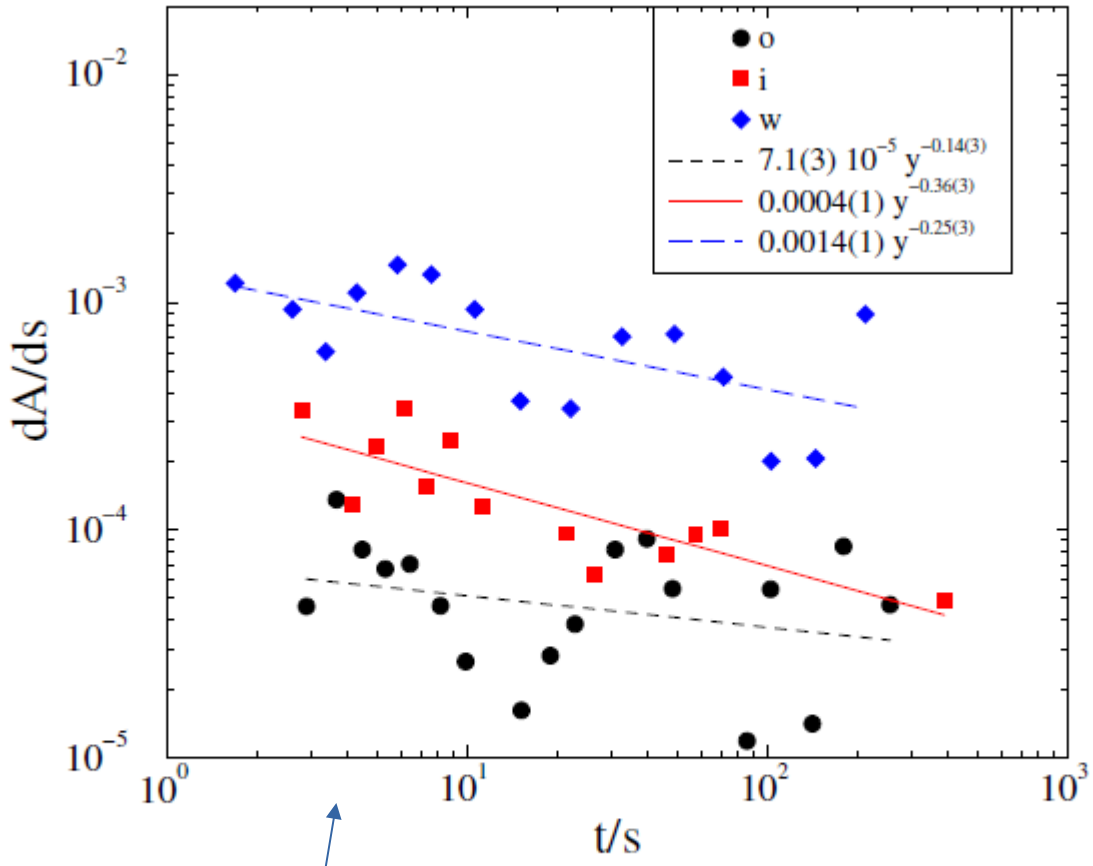

FIG. 9. Summary of the s derivatives of the critical auto-correlation functions: $\dot{A}(t,s)$ for scenarios (o) (bullets), (i) (boxes) and (w) (rhombes), deduced from the largest time results: $t = 258$ and 516 displayed by the legends. Lines show power law fittings assuming $A_0 \times y^{A_1}$ forms for scenarios: (o), (i), (w) (bottom to top curves)

$$\mathcal{R}(t,s) = \frac{1}{T} X(t,s) \frac{\partial A(t,s)}{\partial s}$$

Conclusions

Conclusions

Autocorrelators suffer from large oscillations still PL fitted

Conclusions

Autocorrelators suffer from large oscillations still PL fitted

Autoresponses exhibit scaling collapses, aging exponents obtained

Conclusions

Autocorrelators suffer from large oscillations still PL fitted

Autoresponses exhibit scaling collapses, aging exponents obtained

Violation measure $X(t,s)$ follows the sequence of anisotropy

Conclusions

Autocorrelators suffer from large oscillations still PL fitted

Autoresponses exhibit scaling collapses, aging exponents obtained

Violation measure $X(t,s)$ follows the sequence of anisotropy

Sensitivity is maximal in resting state of the brain

Conclusions

Autocorrelators suffer from large oscillations still PL fitted

Autoresponses exhibit scaling collapses, aging exponents obtained

Violation measure $X(t,s)$ follows the sequence of anisotropy

Sensitivity is maximal in resting state of the brain

Hurst and beta exponents are network community dependent

In agreement with recent fMRI measurements → qualitatively

Conclusions

Autocorrelators suffer from large oscillations still PL fitted

Autoresponses exhibit scaling collapses, aging exponents obtained

Violation measure $X(t,s)$ follows the sequence of anisotropy

Sensitivity is maximal in resting state of the brain

Hurst and beta exponents are network community dependent

In agreement with recent fMRI measurements → qualitatively

Good synchronization model used (Shinomoto-Kuramoto)

Conclusions

Autocorrelators suffer from large oscillations still PL fitted

Autoresponses exhibit scaling collapses, aging exponents obtained

Violation measure $X(t,s)$ follows the sequence of anisotropy

Sensitivity is maximal in resting state of the brain

Hurst and beta exponents are network community dependent

In agreement with recent fMRI measurements → qualitatively

Good synchronization model used (Shinomoto-Kuramoto)

Opens up possibility to predict clinical data

Conclusions

Autocorrelators suffer from large oscillations still PL fitted

Autoresponses exhibit scaling collapses, aging exponents obtained

Violation measure $X(t,s)$ follows the sequence of anisotropy

Sensitivity is maximal in resting state of the brain

Hurst and beta exponents are network community dependent

In agreement with recent fMRI measurements → qualitatively

Good synchronization model used (Shinomoto-Kuramoto)

Opens up possibility to predict clinical data

Publications:

Géza Ódor, István Papp, Shengfeng Deng and Jeffrey Kelling
Synchronization transitions on connectome graphs with external force.
Front. Phys. 11 (2023) 1150246.

Géza Ódor, Istvan Papp and Gustavo Deco
Fluctuation-dissipation of the Kuramoto model on fruit-fly connectomes
ArXiv:2503.20708

HUN REN

Conclusions

Autocorrelators suffer from large oscillations still PL fitted

Autoresponses exhibit scaling collapses, aging exponents obtained

Violation measure $X(t,s)$ follows the sequence of anisotropy

Sensitivity is maximal in resting state of the brain

Hurst and beta exponents are network community dependent

In agreement with recent fMRI measurements → qualitatively

Good synchronization model used (Shinomoto-Kuramoto)

Opens up possibility to predict clinical data

Publications:

Géza Ódor, István Papp, Shengfeng Deng and Jeffrey Kelling
Synchronization transitions on connectome graphs with external force.
Front. Phys. 11 (2023) 1150246.

Géza Ódor, Istvan Papp and Gustavo Deco
Fluctuation-dissipation of the Kuramoto model on fruit-fly connectomes
ArXiv:2503.20708

HUN REN

Conclusions

Autocorrelators suffer from large oscillations still PL fitted

Autoresponses exhibit scaling collapses, aging exponents obtained

Violation measure $X(t,s)$ follows the sequence of anisotropy

Sensitivity is maximal in resting state of the brain

Hurst and beta exponents are network community dependent

In agreement with recent fMRI measurements → qualitatively

Good synchronization model used (Shinomoto-Kuramoto)

Opens up possibility to predict clinical data

Publications:

Géza Ódor, István Papp, Shengfeng Deng and Jeffrey Kelling
Synchronization transitions on connectome graphs with external force.
Front. Phys. 11 (2023) 1150246.

Géza Ódor, Istvan Papp and Gustavo Deco
Fluctuation-dissipation of the Kuramoto model on fruit-fly connectomes
ArXiv:2503.20708

HUN REN

Conclusions

Autocorrelators suffer from large oscillations still PL fitted

Autoresponses exhibit scaling collapses, aging exponents obtained

Violation measure $X(t,s)$ follows the sequence of anisotropy

Sensitivity is maximal in resting state of the brain

Hurst and beta exponents are network community dependent

In agreement with recent fMRI measurements → qualitatively

Good synchronization model used (Shinomoto-Kuramoto)

Opens up possibility to predict clinical data

Publications:

Géza Ódor, István Papp, Shengfeng Deng and Jeffrey Kelling
Synchronization transitions on connectome graphs with external force.
Front. Phys. 11 (2023) 1150246.

Géza Ódor, Istvan Papp and Gustavo Deco
Fluctuation-dissipation of the Kuramoto model on fruit-fly connectomes
ArXiv:2503.20708

HUN REN

Conclusions

Autocorrelators suffer from large oscillations still PL fitted

Autoresponses exhibit scaling collapses, aging exponents obtained

Violation measure $X(t,s)$ follows the sequence of anisotropy

Sensitivity is maximal in resting state of the brain

Hurst and beta exponents are network community dependent

In agreement with recent fMRI measurements → qualitatively

Good synchronization model used (Shinomoto-Kuramoto)

Opens up possibility to predict clinical data

Publications:

Géza Ódor, István Papp, Shengfeng Deng and Jeffrey Kelling
Synchronization transitions on connectome graphs with external force.
Front. Phys. 11 (2023) 1150246.

Géza Ódor, Istvan Papp and Gustavo Deco
Fluctuation-dissipation of the Kuramoto model on fruit-fly connectomes
ArXiv:2503.20708

HUN REN

Conclusions

Autocorrelators suffer from large oscillations still PL fitted

Autoresponses exhibit scaling collapses, aging exponents obtained

Violation measure $X(t,s)$ follows the sequence of anisotropy

Sensitivity is maximal in resting state of the brain

Hurst and beta exponents are network community dependent

In agreement with recent fMRI measurements → qualitatively

Good synchronization model used (Shinomoto-Kuramoto)

Opens up possibility to predict clinical data

Publications:

Géza Ódor, István Papp, Shengfeng Deng and Jeffrey Kelling
Synchronization transitions on connectome graphs with external force.
Front. Phys. 11 (2023) 1150246.

Géza Ódor, Istvan Papp and Gustavo Deco
Fluctuation-dissipation of the Kuramoto model on fruit-fly connectomes
ArXiv:2503.20708

HUN REN

Conclusions

Autocorrelators suffer from large oscillations still PL fitted

Autoresponses exhibit scaling collapses, aging exponents obtained

Violation measure $X(t,s)$ follows the sequence of anisotropy

Sensitivity is maximal in resting state of the brain

Hurst and beta exponents are network community dependent

In agreement with recent fMRI measurements → qualitatively

Good synchronization model used (Shinomoto-Kuramoto)

Opens up possibility to predict clinical data

Publications:

Géza Ódor, István Papp, Shengfeng Deng and Jeffrey Kelling
Synchronization transitions on connectome graphs with external force.
Front. Phys. 11 (2023) 1150246.

Géza Ódor, Istvan Papp and Gustavo Deco
Fluctuation-dissipation of the Kuramoto model on fruit-fly connectomes
ArXiv:2503.20708

HUN REN

Conclusions

Autocorrelators suffer from large oscillations still PL fitted

Autoresponses exhibit scaling collapses, aging exponents obtained

Violation measure $X(t,s)$ follows the sequence of anisotropy

Sensitivity is maximal in resting state of the brain

Hurst and beta exponents are network community dependent

In agreement with recent fMRI measurements → qualitatively

Good synchronization model used (Shinomoto-Kuramoto)

Opens up possibility to predict clinical data

Publications:

Géza Ódor, István Papp, Shengfeng Deng and Jeffrey Kelling
Synchronization transitions on connectome graphs with external force.
Front. Phys. 11 (2023) 1150246.

Géza Ódor, Istvan Papp and Gustavo Deco
Fluctuation-dissipation of the Kuramoto model on fruit-fly connectomes
ArXiv:2503.20708

HUN REN

Conclusions

Autocorrelators suffer from large oscillations still PL fitted

Autoresponses exhibit scaling collapses, aging exponents obtained

Violation measure $X(t,s)$ follows the sequence of anisotropy

Sensitivity is maximal in resting state of the brain

Hurst and beta exponents are network community dependent

In agreement with recent fMRI measurements → qualitatively

Good synchronization model used (Shinomoto-Kuramoto)

Opens up possibility to predict clinical data

Publications:

Géza Ódor, István Papp, Shengfeng Deng and Jeffrey Kelling
Synchronization transitions on connectome graphs with external force.
Front. Phys. 11 (2023) 1150246.

Géza Ódor, Istvan Papp and Gustavo Deco
Fluctuation-dissipation of the Kuramoto model on fruit-fly connectomes
ArXiv:2503.20708

HUN REN